Multiple pendulum and nonuniform distribution of average kinetic energy

Tetsuro Konishi [*]
College of Engineering, Chubu University, Kasugai 487-8501, Japan

Tatsuo Yanagita [†]
Department of Engineering Science, Osaka Electro-Communication University, Neyagawa 572-8530, Japan

(Received 26 May 2023; accepted 9 June 2023; published 10 July 2023)

Multiple pendulums are investigated numerically and analytically to clarify the nonuniformity of average kinetic energies of particles. The nonuniformity is attributed to the system having holonomic constraints and it is consistent with the generalized principle of the equipartition of energy. With the use of explicit expression for Hamiltonian of a multiple pendulum, approximate expressions for temporal and statistical average of kinetic energies are obtained, where the average energies are expressed in terms of masses of particles. In a typical case, the average kinetic energy is large for particles near the end of the pendulum and small for those near the root. Moreover, the exact analytic expressions for the average kinetic energy of the particles are obtained for a double pendulum.

DOI: 10.1103/PhysRevE.108.014204

I. INTRODUCTION

Pendulums are useful to explore the fundamental behavior of various physical systems. A simple pendulum is a good example of a system that can demonstrate periodic motion [1]. When the amplitude of the oscillation is small, i.e., the total energy is small, the periodic motion of a simple pendulum is well approximated by that of a harmonic oscillator, wherein the period of the oscillation does not depend on the amplitude [2].

The fundamental modes and principle of superposition can be understood by studying a double pendulum [2–5]. When the amplitude of oscillation is small, there are two special motions called the fundamental modes, wherein both the upper and lower pendulums oscillate in the same period. For a small-amplitude oscillation, one can understand that every motion of the double pendulum is expressed by the superposition of the two fundamental modes. The principle of superposition is a key concept for understanding various linear phenomena. Since both fundamental modes of the double pendulum are periodic motion, the double pendulum exhibits periodic or quasiperiodic motion when the amplitudes are small.

Meanwhile, a double pendulum is also a good example of a system that exhibits chaotic motion [6–17]. If a large energy is assigned and the amplitudes of displacements are not small, then the motion of a double pendulum is no longer regular, and chaotic behavior is observed. Multiple pendulums with three or more degrees of freedom [3–5] also exhibit chaotic behavior [18–20].

When chaos is strong in a multiple pendulum, one can expect that it admits a statistical description; the long-time average of the physical quantity is considered to be approximately equal to the average over the energy surface. Then, each particle in the pendulum can be considered as a subsystem connected to a heat bath that comprises the rest of the pendulum; then the particles behave as if they are in thermal equilibrium.

One may expect that the system in thermal equilibrium is almost uniform. However, a careful observation of the motions of a multiple pendulum indicate that the particle at the end of the pendulum moves faster than the particle nearest to the root of the pendulum, even if the masses of all particles are the same. In fact, one author conducted numerical computations and revealed that the time averages of the kinetic energies of a multiple pendulum are different [18–20]. In this paper, we revisit the observation and explain the origin of differences in the average kinetic energies using the generalized principle of the equipartition of energy [21–24]. The nonuniformity of the average kinetic energy is consistent with the generalized principle of equipartition of energy. Thus, the average kinetic energy can be nonuniform under a thermal equilibrium.

The remainder of this paper is organized as follows. In Sec. II, we describe our model, a multiple pendulum. Then we provide an explicit form of the Lagrangian and Hamiltonian of a multiple pendulum. In Sec. III, we present the results of numerical computation where the values of time-average kinetic energies of particles in the multiple pendulum are not equal. In Sec. IV, we show that the nonuniformity is also found for statistical average, and the nonuniformity of temporal and statistical averages agree quite well. Then we explain the nonuniform distribution of average kinetic energy based on statistical mechanics and the generalized principle of the equipartition of energy; further, an exact expression is obtained for the double pendulum. Finally, Sec. V presents the summary and the discussions.

[*] tkonishi@isc.chubu.ac.jp
[†] yanagita@osakac.ac.jp

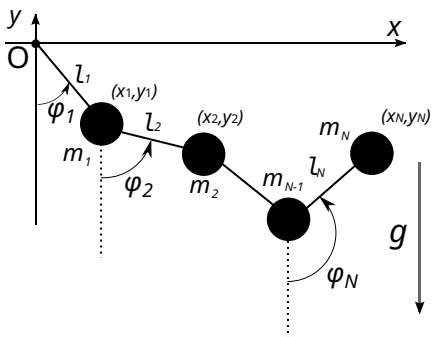

FIG. 1. Multiple pendulum: Definition of variables and parameters.

II. MODEL

The multiple pendulum examined in this study is composed of N particles serially connected by N massless links of fixed length in a uniform gravitational field, as illustrated in Fig. 1. One end is fixed to a point we define as the origin (0,0). The particles and links pass through each other if they arrive at the same position. The particles move in a fixed vertical plane, which is defined as the xy plane. The x axis is considered to be in the horizontal direction, and the y axis is in the vertical direction, with the upward direction representing the positive y direction. We let m_i, $\overrightarrow{r_i} = (x_i, y_i)$, and ℓ_i represents the mass of the ith particle, position of the ith particle, and length of ith link, respectively. g represents the constant of gravitational acceleration. The distance between ith and $i+1$th particles is fixed for all i. In this sense, the system has holonomic constraints.

In terms of the Cartesian coordinates (x_i, y_i), the kinetic energy of the ith particle K_i, total kinetic energy K, and potential energy U are

$$K_i = \frac{m_i}{2}\left(\dot{x}_i^2 + \dot{y}_i^2\right), \tag{1}$$

$$K = \sum_{i=1}^{N} K_i, \tag{2}$$

$$U = \sum_{i=1}^{N} m_i g y_i, \tag{3}$$

where a dot over each symbol represents derivative with respect to time, e.g., $\dot{x}_i = \frac{dx_i}{dt}$.

Using these equations, the system is defined by a Lagrangian L and constraints G_i, which are given as

$$L = K - U = \sum_{i=1}^{N} \frac{m_i}{2}\left(\dot{x}_i^2 + \dot{y}_i^2\right) - \sum_{i=1}^{N} m_i g y_i, \tag{4}$$

$$G_i = |\overrightarrow{r_i} - \overrightarrow{r_{i-1}}|^2 - \ell_i^2 = 0, \quad i = 1, 2, \ldots, N, \tag{5}$$

where $\overrightarrow{r_0} = (x_0, y_0) = (0, 0)$.

If we denote φ_i as the angle between the ith link and the $-y$ direction (direction of gravity) as shown in Fig. 1, then we have

$$x_i = x_{i-1} + \ell_i \sin\varphi_i = \sum_{j=1}^{i} \ell_j \sin\varphi_j, \tag{6}$$

$$y_i = y_{i-1} - \ell_i \cos\varphi_i = -\sum_{j=1}^{i} \ell_j \cos\varphi_j. \tag{7}$$

The Lagrangian Eq. (4) is then expressed in terms of φ_i, $i = 1, 2, \ldots, N$ as

$$L = K - U, \tag{8}$$

$$K = \sum_{i,j=1}^{N} \frac{1}{2} A(\varphi)_{ij} \dot{\varphi}_i \dot{\varphi}_j = \frac{1}{2}\,{}^t\dot{\varphi} A(\varphi) \dot{\varphi}, \tag{9}$$

$$U = -\sum_{i=1}^{N} m_i g \sum_{j=1}^{i} \ell_j \cos\varphi_j, \tag{10}$$

where $\dot{\varphi}$ without subscript is a vector composed of N elements

$$\dot{\varphi} = {}^t(\dot{\varphi}_1, \ldots, \dot{\varphi}_N), \tag{11}$$

and the symbol "t" represents transpose, and the elements of $N \times N$ matrix A is defined as

$$A(\varphi)_{nk} = \left[\sum_{i=\max(n,k)}^{N} m_i\right] \ell_n \ell_k \cos(\varphi_n - \varphi_k). \tag{12}$$

The derivations of Eqs. (9) and (12) are presented in Appendix A.

Using Eqs. (6) and (7), K_i [Eq. (1)] can be expressed in the quadratic form of $\dot{\varphi}$ as

$$K_i = \frac{m_i}{2} \sum_{j=1}^{i} \sum_{k=1}^{i} \dot{\varphi}_j \dot{\varphi}_k \ell_j \ell_k \cos(\varphi_j - \varphi_k) \tag{13}$$

$$= \frac{1}{2} \sum_{j,k} A_{jk}^{(i)} \dot{\varphi}_j \dot{\varphi}_k = \frac{1}{2}\,{}^t\dot{\varphi} A^{(i)} \dot{\varphi}, \tag{14}$$

where $A^{(i)}$ represents a $N \times N$ matrix defined as

$$A_{jk}^{(i)} = \begin{cases} m_i \ell_j \ell_k \cos(\varphi_j - \varphi_k) & \cdots j \leqslant i \text{ and } k \leqslant i, \\ 0 & \cdots \text{otherwise.} \end{cases} \tag{15}$$

Because $\sum_{i=1}^{N} K_i = K$, the sum of $A^{(i)}$ with respect to i is equal to the matrix A:

$$\sum_{i=1}^{N} A_{jk}^{(i)} = A_{jk}. \tag{16}$$

Note that matrices A and $A^{(i)}$ depend on coordinates φ.

The momentum p_i canonically conjugate to the coordinate φ_i is defined as

$$p_i = \frac{\partial L}{\partial \dot{\varphi}_i}. \tag{17}$$

Then, we have

$$p_n = \sum_{k=1}^{N} A_{nk} \dot{\varphi}_k = (A\dot{\varphi})_n, \tag{18}$$

$$K = \frac{1}{2} \sum_{j,k} p_j A_{jk}^{-1} p_k = \frac{1}{2}\,{}^t p A^{-1} p, \tag{19}$$

$$K_i = \frac{1}{2}\sum_{j,k,\xi,\eta} A^{(i)}_{jk} A^{-1}_{j\xi} A^{-1}_{k\eta} p_\xi p_\eta = \frac{1}{2}{}^t p A^{-1} A^{(i)} A^{-1} p. \quad (20)$$

Here p without subscript is

$$p = {}^t(p_1, \ldots, p_N).$$

Using Eq. (19), the Hamiltonian of a multiple pendulum is given as

$$H = \frac{1}{2}{}^t p A^{-1} p - \sum_{i=1}^{N} m_i g \sum_{j=1}^{i} \ell_j \cos\varphi_j. \quad (21)$$

III. DYNAMICAL BEHAVIOR AND ANALYSIS

In this section, we study the temporal average of kinetic energy of each particle by numerically integrating the equation of motion. Then we reproduce the results by Yanagita *et al.* [18–20] about the nonuniformity of average kinetic energy and interpret the results.

A. Simulation method

First, let us explain the method of numerical simulation using which we integrate the equation of motion of the multiple pendulum. The equation of motion derived from the Lagrangian written in terms of φ is complicated because of the dependence of the kinetic energy on φ. Hence, we use the equation of motion written in terms of the Cartesian coordinates x and y derived from Eqs. (4) and (5). The equation of motion includes the terms from the holonomic constraints characterized by the coefficients called "Lagrange multipliers" [2]. We numerically evaluate the Lagrange multipliers at each step of the integration to ensure that the constraints in Eq. (5) are satisfied. The idea used in this method is the same as that in the "RATTLE" algorithm [25–27]. We use the fourth-order symplectic integrator composed of three second-order symplectic integrators [25,28] incorporating forces from the holonomic constraints.

We calculate the kinetic energies of the particles of the multiple pendulum. Let us denote $K_i(t)$ as the kinetic energy of the ith particle [Eq. (1)] at time t. The time average of $K_i(t)$ is defined as

$$\overline{K_i}(t) = \frac{1}{t}\int_0^t K_i(t')\,dt'. \quad (22)$$

B. Simulation results

Let us observe some typical time evolutions of the multiple pendulum obtained from the numerical simulation. Here we adopt the initial condition $\dot{x}_i(0) = \dot{y}_i(0) = 0$ for all i; $\varphi_i(0) = \varphi_0$ for all i. This is a stretched configuration with angle φ_0.

Let us consider the initial angle as $\varphi_0 = \pi/2$. The top panel of Fig. 2 shows the chaotic motion after a short transient; the bottom panel shows the temporal evolution of the average kinetic energies $\overline{K_i}(t)$. We see that $\overline{K_i}(t)$ does not converge to a single value; on the contrary, they converge to different values, i.e., the average kinetic energy is not uniform.

In Fig. 3, we show the convergence of $\overline{K_i}(t)$. We see that

$$|\overline{K_i}(t) - \overline{K_i}(t_{\max})| \approx \frac{1}{t} \quad (23)$$

for each i.

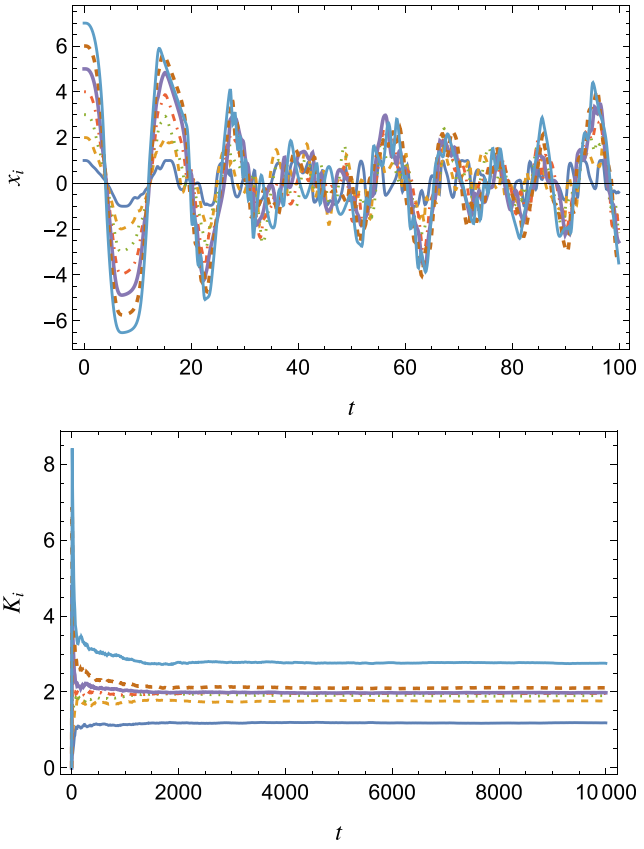

FIG. 2. (top): Time evolution of a multiple pendulum. The horizontal axis represents time, and the vertical axis represents the x coordinate of each particle $x_i(t)$. $N = 7$, $m_i = 1$, and $\ell_i = 1$ for all i; $g = 1$. The time step for the numerical integration is $\Delta t = 0.001$. The initial conditions are $\varphi_i = \frac{\pi}{2}$ and $\dot{\varphi}_i = 0$ for all i. (bottom): Average kinetic energies $\overline{K_i}(t)$ vs t calculated from the time evolution shown in the top panel. The lines represent $\overline{K_1}(t)$, $\overline{K_2}(t)$, …, and $\overline{K_7}(t)$, from the bottom to the top.

Figure 4 shows a plot of the average kinetic energy of each particle $\overline{K_i}(t_{\max})$ [Eq. (22)] against i for $N = 7$. Note that the values of $\overline{K_i}(t_{\max})$ are not the same. That is, the $\overline{K_i}(t_{\max})$ of

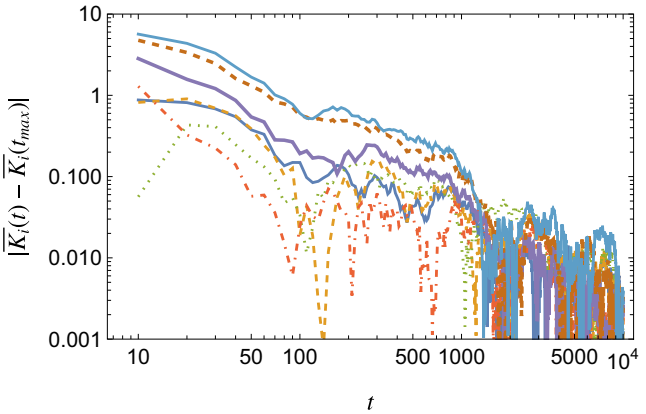

FIG. 3. Convergence of $|\overline{K_i}(t) - \overline{K_i}(t_{\max})|$ for the values of $\overline{K_i}(t)$ shown in Fig. 2, where $t_{\max} = 10^4$. The time averages converge approximately as $1/t$.

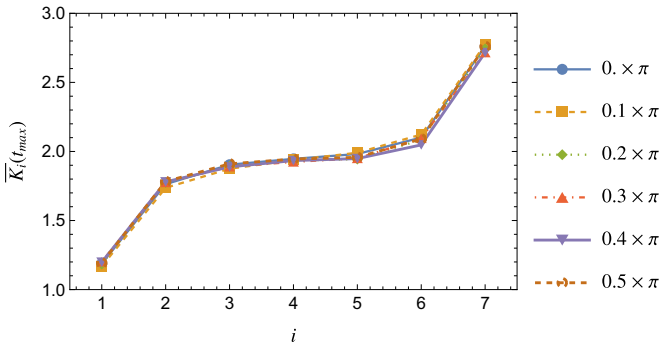

FIG. 4. Long-time average of kinetic energy $\overline{K_i}(t_{\max})$ vs i for six different initial conditions which have the same total energy. $N = 7$, $m_i = 1$, and $\ell_i = 1$ for all i; $g = 1$. $t_{\max} = 1.0 \times 10^4$. The initial condition is $\varphi_i = \varphi_0$ for all i, and $\varphi_0 = 0,\ 0.1\pi,\ 0.2\pi, \ldots, 0.5\pi$. Initial angle velocity is $\dot{\varphi}_i = \dot{\varphi}_0$ for all i. $\dot{\varphi}_0$ is determined as follows; For $\varphi_0 = 0.5\pi$, $\dot{\varphi}_0 = 0$. For $\varphi_0 \neq 0.5\pi$, $\dot{\varphi}_0$ is determined as the total energy $E_{\text{total}}(\varphi_0, \dot{\varphi}_0)$ is the same as the case $\varphi_0 = 0.5\pi$, i.e., $E_{\text{total}}(\varphi_0, \dot{\varphi}_0) = E_{\text{total}}(\varphi_0 = 0.5\pi, 0)$.

particles near the end are large, whereas those of particles near the root are small. This is consistent with Yanagita *et al.*'s first observation [18–20].

We observed that the time averages of kinetic energies of particles converged through chaotic motion. Let us examine the property of chaotic dynamics by measuring Lyapunov exponents. Figure 5 represents the Lyapunov exponents and spectra for a multiple pendulum for several initial conditions. Details of the numerical methods of the calculation are shown in Appendix B. In Fig. 5(a) we show the Lyapunov spectra for $N = 7$. The initial condition is $\varphi_i = \varphi_0$, $\dot{\varphi}_i = 0$ for all i, which include the one used for calculating Fig. 2. For Hamiltonian systems the Lyapunov exponents λ_i show a symmetry $\lambda_i + \lambda_{2N+1-i} = 0$, we see that the system is fully chaotic except for $\varphi_0 = \pi/4$. Figure 5(b) shows the initial angle dependence of the sum of positive Lyapunov exponents. When φ_0 is small the system shows regular oscillation, and above a critical value of φ_0 the system becomes fully chaotic. The onset of chaotic behavior depends on the system size. We show in Fig. 5(c) the maximum Lyapunov exponent λ_1 vs the initial angle φ_0. As the system size increases, the value of φ_0 at the onset of chaotic behavior becomes small.

C. Analysis on temporal average

We see that the long-time average of kinetic energy of each particle $\overline{K_i}(t)$ does not converge to the same value. Since the nonuniformity is observed in the data obtained from dynamics, one may think that the origin of the nonuniformity lies in nonergodic behavior, e.g., the orbit does not evenly visit the energy surface because of existence of KAM tori or their remnants. However, the nonuniformity arises even when the system is highly chaotic. Hence we interpret the nonuniformity as a result of almost random behavior of the dynamics.

Let us introduce quantities $K_i^{(c)}$ defined as

$$K_i^{(c)} = \frac{1}{2} p_i \frac{\partial H}{\partial p_i}, \quad i = 1, 2, \ldots, N, \tag{24}$$

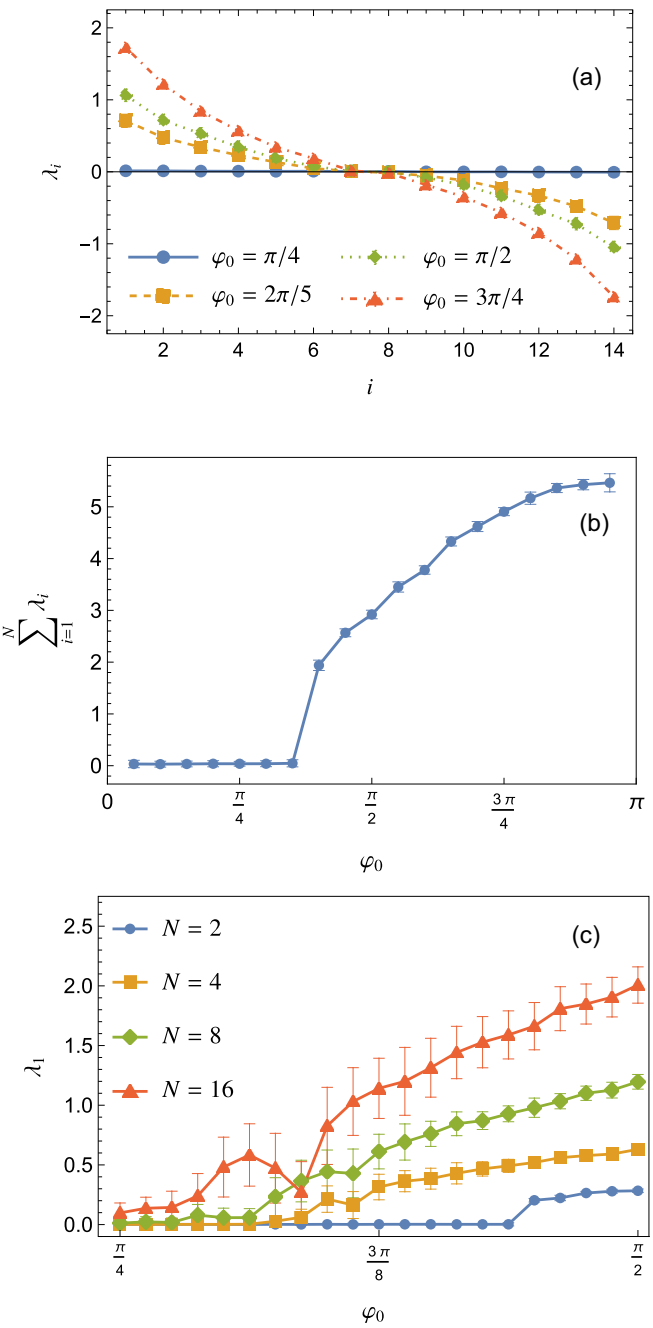

FIG. 5. (a) The Lyapunov spectrum of a multiple pendulum: $N = 7$. Initial condition is $\varphi_i = \varphi_0$ and $\dot{\varphi}_i = 0$ for all i, and $\varphi_0 = \pi/4$, $2\pi/5$, $\pi/2$, $3\pi/4$. (b) Dependence of the sum of positive Lyapunov exponents $\sum_{i=1}^{N} \lambda_i$ on the initial angle φ_0. (c) The maximum Lyapunov exponent for various system sizes $N = 2, 4, 8, 16$.

where p_i is the momentum conjugate to φ_i, and the sum over repeated index i is not taken. We call $K_i^{(c)}$ as "canonical kinetic energy."

For a multiple pendulum $K_i^{(c)}$ is expressed as

$$K_i^{(c)} = \sum_{j=1}^{N} \frac{1}{2} \left[\sum_{n=\max(i,j)}^{N} m_n \right] [\Delta \dot{x}_i \Delta \dot{x}_j + \Delta \dot{y}_i \Delta \dot{y}_j], \tag{25}$$

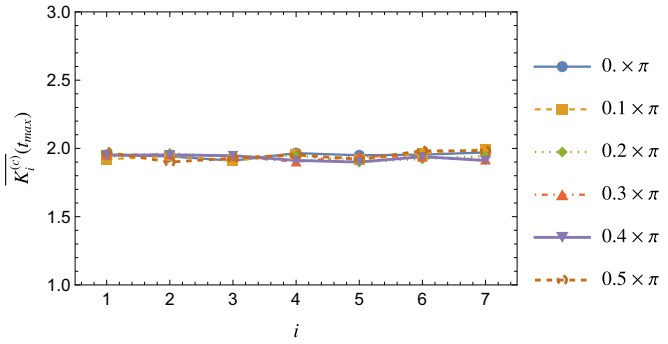

FIG. 6. Long-time average of canonical kinetic energy $\overline{K_i^{(c)}}(t_{\max})$ Eq. (27) vs i. This plot is obtained using the same time series as that in Fig. 4.

where

$$\Delta x_i = x_i - x_{i-1}, \quad \Delta y_i = y_i - y_{i-1}. \tag{26}$$

and $\Delta\dot{x}_1 = \dot{x}_1$, $\Delta\dot{y}_1 = \dot{y}_1$ because $x_0 = y_0 = 0$. The detail of calculation is shown in Appendix C.

Figure 6 shows $\overline{K_i^{(c)}}(t_{\max})$, the time average of canonical kinetic energy, Eq. (24), of the multiple pendulum using the same time series as in Fig. 4, defined as

$$\overline{K_i^{(c)}}(t_{\max}) = \frac{1}{t_{\max}} \int_0^{t_{\max}} K_i^{(c)}(t)dt. \tag{27}$$

We see that $\overline{K_i^{(c)}}(t_{\max})$ take almost the same value for all i.

Let us derive the nonuniform distribution of $\overline{K_i}$. For this purpose let us assume

$$\overline{\Delta\dot{x}_i\Delta\dot{x}_j} \approx 0, \quad \overline{\Delta\dot{y}_i\Delta\dot{y}_j} \approx 0 \ \ (i \neq j). \tag{28}$$

This assumption implies that each link in the multiple pendulum rotates statistically independently. Since the nonuniformity of the average kinetic energy is observed when the system behaves in a highly chaotic manner, this assumption is reasonable.

Then, we have by straightforward calculation that

$$\overline{K_i^{(c)}} \approx \frac{1}{2}\left(\sum_{n=i}^{N} m_n\right)\left[\left(\overline{\dot{x}_i^2} + \overline{\dot{y}_i^2}\right) - \left(\overline{\dot{x}_{i-1}^2} + \overline{\dot{y}_{i-1}^2}\right)\right] \tag{29}$$

$$= \left(\sum_{n=i}^{N} m_n\right)\left(\frac{1}{m_i}\overline{K_i} - \frac{1}{m_{i-1}}\overline{K_{i-1}}\right). \tag{30}$$

In Fig. 6, $\overline{K_i^{(c)}}$ is almost uniform over the system. In fact, we see in the later section that the thermal average of $K_i^{(c)}$ is equal to $\frac{1}{2}k_BT$ by the generalized principle of equipartition of energy. See Appendix D for details. Hence let us assume that $\overline{K_i^{(c)}}$ does not depend on i and write the value as

$$\overline{K_i^{(c)}} = \overline{K^{(c)}} \tag{31}$$

for all i.

Then the long-time average of kinetic energy of the ith particle K_i is recursively expressed as

$$\overline{K_i} \approx \frac{m_i}{m_{i-1}}\overline{K_{i-1}} + \frac{m_i}{\sum_{n=i}^{N} m_n} \cdot \overline{K^{(c)}}. \tag{32}$$

Since $(x_0, y_0) = (0, 0)$ and $K_0 = 0$, we have

$$\overline{K_i} \approx m_i\left(\sum_{j=1}^{i} \frac{1}{\sum_{n=i}^{N} m_n}\right) \cdot \overline{K^{(c)}}. \tag{33}$$

Hence, the temporal average of the kinetic energy is nonuniform.

If all masses have the same value $m_1 = m_2 = \cdots = m_N$, then $\overline{K_n}$'s are explicitly expressed as

$$\overline{K_i} \approx \left(\sum_{j=1}^{i} \frac{1}{N - j + 1}\right)\overline{K^{(c)}}, \tag{34}$$

so that the average linear kinetic energies $\overline{K_i}$ can monotonically increase from the root to the end of the pendulum as

$$\overline{K_1} < \overline{K_2} < \cdots < \overline{K_N}. \tag{35}$$

This is consistent with the numerical results shown in Fig. 4.

IV. STATISTICAL BEHAVIOR AND ANALYSIS

In the previous section, we see that $\overline{K_i}$, the long-time average of kinetic energy of each particle in a multiple pendulum in chaotic motion, does not take the same value. When all the masses are the same and length of all the links are the same, average kinetic energy of a particle is small if the particle is near the root and is large if it is near the end of the pendulum. The behavior is observed when the motion of the pendulum is fully chaotic. Contrary to a naive expectation that the average kinetic energy is uniform over the system, nonuniformity appeared.

Let us examine the origin of the nonuniformity. Since the nonuniformity appears in the temporal average of kinetic energy $\overline{K_i}$, one may guess that a possible cause lies in dynamical effect and nonergodic behavior, e.g., existence of KAM tori or their remnants, and nonergodic behavior may make the chaotic time series different from the behavior in thermal equilibrium. Hence let us compare the time average $\overline{K_i}$ and statistical average $\langle K_i\rangle$. As the statistical average, here we adopt canonical average instead of microcanonical average, since it is much easier to calculate. If the difference between $\overline{K_i}$ and $\langle K_i\rangle$ is large or small, then we can think of the origin of nonuniformity as dynamical or statistical.

Figure 7 shows the temporal and statistical average kinetic energies of a multiple pendulum of $N = 16$. Here we show time average $\overline{K_i}$ defined as Eq. (22) and statistical average $\langle K_i\rangle$ defined as

$$\langle K_i\rangle = \frac{1}{Z}\int K_i(q, p)e^{-\beta H}d\Gamma, \tag{36}$$

where Z is the partition function $Z = \int e^{-\beta H}d\Gamma$, $\beta = 1/k_BT$, T is the temperature, k_B is Boltzmann's constant, and $d\Gamma = d^Np\,d^N\varphi$. $\overline{K_i}$ is the same as shown in Fig. 4. $\langle K_i\rangle$ is obtained from Markov-chain Monte Carlo (MCMC) simulation. β in Eq. (36) is defined as follows. Given a total kinetic energy $\sum_{i=1}^{N}\overline{K_i}$, the value of β used in Fig. 7 for $\langle K_i\rangle$ is implicitly determined from the following equation:

$$\sum_{i=1}^{N}\langle K_i\rangle = \sum_{i=1}^{N}\overline{K_i}. \tag{37}$$

Details of MCMC simulation are described in Appendix E.

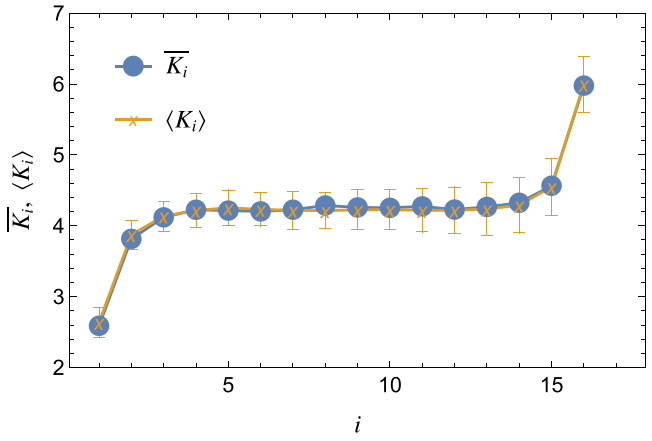

FIG. 7. Comparison between the temporal average of kinetic energy $\overline{K_i}$ obtained from time series, and canonical average $\langle K_i \rangle$ obtained from MCMC simulation.

We see that in Fig. 7 the time average $\overline{K_i}$ and the statistical average $\langle K_i \rangle$ agree quite well. The striking similarity between the time average $\overline{K_i}$ and the statistical average $\langle K_i \rangle$ presents a possible interpretation about the origin of nonuniformity. That is, there is a nonuniformity in the statistical average $\langle K_i \rangle$ shown in Fig 7, and it is reflected to the nonuniformity in the time average $\overline{K_i}$ because the long-time series resembles the statistical ensemble. In other words, the true origin of nonuniformity may be in statistical mechanics of systems with holonomic constraints, not in dynamics.

In the following, we show how to understand the nonuniformity of average energy in thermal equilibrium.

A. Nonuniformity of average dinetic dnergy and the generalized principle of the equipartition of energy

Let us investigate the relationship between the nonuniformity of $\langle K_i \rangle$ we observed in the previous subsection and the generalized principle of the equipartition of energy [21–24]. Equation (9) shows that the kinetic energy of the system has off-diagonal elements that depend on the coordinate φ. Thus, we cannot apply the ordinary form of the principle of the equipartition of energy. Instead, we use the generalized principle of the equipartition of energy, which states

$$\left\langle K_i^{(c)} \right\rangle = \tfrac{1}{2} k_B T. \tag{38}$$

Here T represents the temperature, k_B denotes Boltzmann's constant, the bracket $\langle \cdots \rangle$ represents the thermal average, and $K_i^{(c)}$ is defined as Eq. (24). The generalized principle of the equipartition of energy is summarized in Appendix D. We call K_i and $K_i^{(c)}$ the "linear kinetic energy" and "canonical kinetic energy," respectively.

For the multiple pendulum, $K_i^{(c)}$ is

$$K_i^{(c)} = \sum_{k=1}^{N} \frac{1}{2} p_i A^{-1}_{ik} p_k = p_i \dot{\varphi}_i. \tag{39}$$

This is different from the kinetic energy of the ith particle K_i defined in Eq. (20), i.e., $K_i \neq K_i^{(c)}$, hence

$$\langle K_i \rangle \neq \left\langle K_i^{(c)} \right\rangle = \tfrac{1}{2} k_B T. \tag{40}$$

As an example, $K_i^{(c)}$ for the case of double pendulum is shown in Appendix C 1. Using Eqs. (38) and (40), $\langle K_i \rangle$, the average of K_i, does not take the same value at the thermal equilibrium in general.

Remember that in Fig. 6, $\overline{K_i^{(c)}}$ takes almost the same value and the generalized principle of the equipartition of energy is realized. Since $\langle K_i^{(c)} \rangle$ does not depend on i, $\langle K_i \rangle$ may depend on i, i.e., nonuniform. That is, due to the fact that the thermal equilibrium is established and the generalized principle of equipartition of energy holds, the average of K_i takes different values and the nonuniformity of the average kinetic energy is realized in the thermal equilibrium.

B. Analysis on statistical average

Let us explain the nonuniformity of the statistical average of kinetic energy $\langle K_i \rangle$. Suppose the system is under thermal equilibrium at temperature T. The statistical average of the linear kinetic energy K_i is then defined as Eq. (36).

Using the expression for K_i, we have

$$\langle K_i \rangle = \frac{m_i}{2} \sum_{j=1}^{i} \sum_{k=1}^{i} \ell_j \ell_k \langle \dot{\varphi}_j \dot{\varphi}_k \cos \varphi_{jk} \rangle, \tag{41}$$

where $\varphi_{jk} = \varphi_j - \varphi_k$.

Using Eq. (20), we can express Eq. (41) in terms of the canonical momenta p_i as

$$\langle K_i \rangle = \frac{1}{2} \sum_{j,k,\xi,\eta} \left\langle A^{(i)}_{jk} A^{-1}_{j\xi} A^{-1}_{k\eta} p_\xi p_\eta \right\rangle = \left\langle \frac{1}{2}{}^t p A^{-1} A^{(i)} A^{-1} p \right\rangle. \tag{42}$$

Integrating by parts with respect to p yields

$$\langle K_i \rangle = \frac{1}{2\beta} \langle \mathrm{tr}(A^{(i)} A^{-1}) \rangle \tag{43}$$

$$= \frac{1}{2\beta} \frac{1}{Z} \int \mathrm{tr}(A^{(i)} A^{-1}) e^{-\beta[\frac{1}{2} p A^{-1} p + U(\varphi)]} d\Gamma. \tag{44}$$

Here matrices A^{-1} and $A^{(i)}$ depend on φ. Derivation of Eq. (43) is described in Appendix F.

In Eq. (44), we first perform integration with respect to p, which is a multidimensional Gaussian integral. The result is

$$\int e^{-\beta(\frac{1}{2} p A^{-1} p)} d^N p = \left(\frac{2\pi}{\beta} \right)^{N/2} \sqrt{\det A}. \tag{45}$$

Hence, we have

$$Z = \left(\frac{2\pi}{\beta} \right)^{N/2} \int \sqrt{\det A}\, e^{-\beta U(\varphi)} d^N \varphi, \tag{46}$$

$$\langle K_i \rangle = \frac{1}{2\beta} \frac{\int \mathrm{tr}(A^{(i)} A^{-1}) \sqrt{\det A}\, e^{-\beta U(\varphi)} d^N \varphi}{\int \sqrt{\det A}\, e^{-\beta U(\varphi)} d^N \varphi}. \tag{47}$$

These are exact expressions. In the following, we use these equations to express $\langle K_i \rangle$ for multiple and double pendulums.

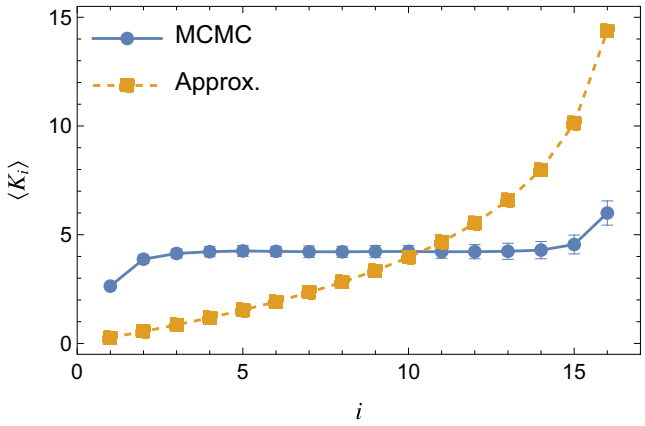

FIG. 8. Comparison of thermal average of kinetic energy $\langle K_i \rangle$, obtained by evaluating Eq. (36) by MCMC simulation (filled circles with solid lines) and obtained by numerically evaluating the approximation Eq. (50) (filled squares with broken lines).

1. Approximate expression for multiple pendulum with an arbitrary number of particles

Let us adopt "diagonal approximation"

$$\langle \dot{\varphi}_j \dot{\varphi}_k \cos \varphi_{jk} \rangle \approx 0 \quad \text{for } j \neq k\,, \tag{48}$$

and

$$\left\langle A^{-1}_{jj} \right\rangle \approx \left\langle \frac{1}{A_{jj}} \right\rangle = \frac{1}{\left(\sum_{i=j}^{N} m_i\right) \ell_j^2}. \tag{49}$$

These approximations assume that each link rotates statistically independently, and we omit all off-diagonal elements of matrix A, where phase factors such as $\cos(\varphi_i - \varphi_j)$ are included.

Then, we obtain

$$\langle K_i \rangle \approx m_i \left(\sum_{j=1}^{i} \frac{1}{\sum_{n=j}^{N} m_n} \right) \cdot \frac{1}{2} k_B T. \tag{50}$$

This expression is equivalent to that in Eq. (33) if the thermal average on the left-hand side $\langle \cdots \rangle$ is replaced by the time average $\overline{\cdots}$ and the generalized principle of equipartition of energy, i.e., Eq. (38) is used. The details of the calculation are summarized in Appendix G.

This result indicates that when all masses are the same, the average linear kinetic energies are monotonically increasing from the root to the end of the pendulum, as shown in Fig. 4.

$$\langle K_1 \rangle < \langle K_2 \rangle < \cdots < \langle K_N \rangle. \tag{51}$$

2. Validity of approximation

Let us examine the validity of the approximate expression Eq. (50) for the average kinetic energy $\langle K_i \rangle$. For that purpose let us compare the approximate expression and $\langle K_i \rangle$ obtained by MCMC simulation. If the approximation Eq. (50) is close to the one by MCMC simulation, then we consider the approximation is valid.

In Fig. 8 we show $\langle K_i \rangle$ obtained by the approximation Eq. (50) and by evaluating the definition Eq. (36) by MCMC simulation. We see that the approximate expression agrees with the result of MCMC simulation in nonuniformity and monotonically increasing behavior, but it fails to express the flat profile in the middle of the pendulum shown by MCMC simulation.

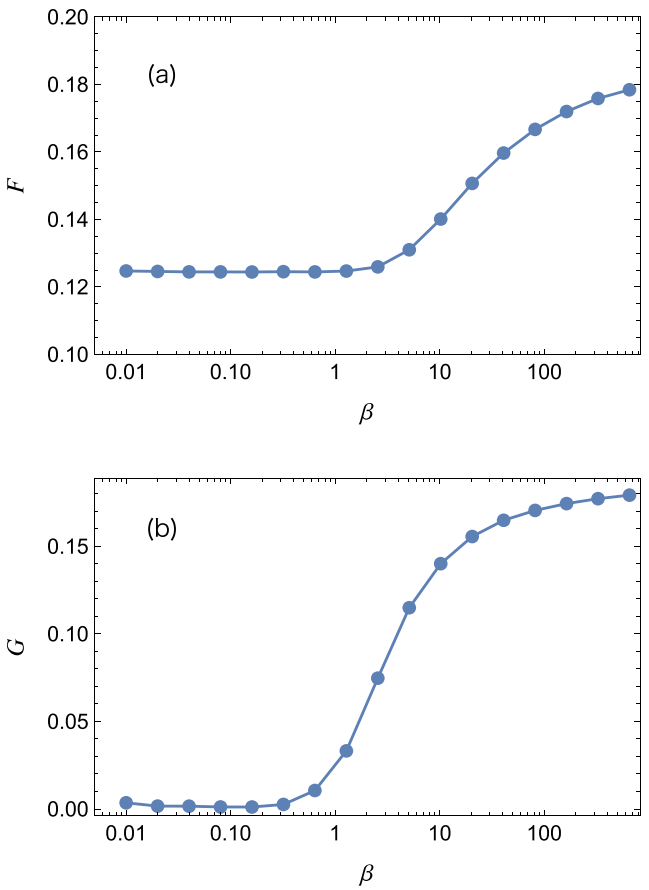

FIG. 9. (a) Values of F [Eq. (52)] as a function of β obtained by MCMC simulation. $N = 16$. (b) Values of G [Eq. (53)] as a function of β obtained by MCMC simulation. $N = 16$.

Let us examine whether the assumptions Eqs. (48) and (49) are valid. By using MCMC simulation we calculate the quantities which are assumed to be zero in the approximations.

We define two quantities F and G as

$$F = \sqrt{\frac{1}{N(N-1)} \sum_{j \neq k} \langle \dot{\varphi}_j \dot{\varphi}_k \cos \varphi_{jk} \rangle^2} \tag{52}$$

and

$$G = \frac{1}{\mathrm{Tr}(A^{-1})/N} \sqrt{\frac{1}{N(N-1)} \sum_{j \neq k} \langle (A^{-1})_{jk} \rangle^2}, \tag{53}$$

where F and G represent the magnitude of quantities assumed to be zero in the approximation Eq. (48) and Eq. (49), respectively.

Figure 9(a) shows the value of F defined by Eq. (52). Each value is obtained by MCMC simulation. This quantity check the validity of the assumption that $\langle \dot{\varphi}_j \dot{\varphi}_k \cos \varphi_{jk} \rangle$ is small. We see that the values remain finite for a wide range of temperature. In particular, the value does not converge to zero even for high temperature.

Figure 9(b) shows the value of G defined by Eq. (53). Each value is obtained by MCMC simulation. This quantity checks the validity of the assumption that off-diagonal elements of the matrix A^{-1} is small. In the figure, we see that the quantities approximated as zero in Eq. (49) remain positive, in particular for large values of β.

In summary, the approximations Eqs. (48) and (49) used to obtain Eq. (50) are useful to describe some of qualitative features, e.g., nonuniform distribution of $\langle K_i\rangle$ and monotonically increasing behavior of $\langle K_i\rangle$ vs i, but the assumptions on which the approximation is based are not completely satisfied as seen in Fig. 9. This incompleteness leads to the discrepancy between the true value and approximated value of of $\langle K_i\rangle$ found in Fig. 8.

3. *Exact expression for double pendulum*

We have obtained approximate expressions for average kinetic energy $\langle K_i\rangle$. The expressions, however, differ from true values; hence it would be appropriate if we could obtain more accurate expressions for $\langle K_i\rangle$.

For the case of the double pendulum, i.e., for the $N = 2$ case, we can obtain the exact expression for $\langle K_i\rangle$. That is, Eq. (47) is exactly evaluated.

For $N = 2$, matrices A, $A^{(i)}$, defined by Eqs. (12) and (15), respectively, and $\det A$ reads

$$A = M\begin{pmatrix} \ell_1^2 & \mu_2\ell_1\ell_2C_{12} \\ \mu_2\ell_1\ell_2C_{12} & \mu_2\ell_2^2 \end{pmatrix}, \tag{54}$$

$$A^{(1)} = M\mu_1\ell_1^2\begin{pmatrix} 1 & 0 \\ 0 & 0 \end{pmatrix}, \tag{55}$$

$$A^{(2)} = M\mu_2\begin{pmatrix} \ell_1^2 & \ell_1\ell_2C_{12} \\ \ell_1\ell_2C_{12} & \ell_2^2 \end{pmatrix}, \tag{56}$$

$$\det A = M^2\mu_2\ell_1^2\ell_2^2\left(1-\mu_2C_{12}^2\right), \tag{57}$$

where

$$C_{12} = \cos(\varphi_2-\varphi_1), \tag{58}$$

$$M = m_1+m_2, \tag{59}$$

$$\mu_i = m_i/M. \tag{60}$$

From these, we obtain

$$\mathrm{tr}(A^{(1)}A^{-1}) = \frac{\mu_1}{1-\mu_2C_{12}^2}, \tag{61}$$

$$\mathrm{tr}(A^{(2)}A^{-1}) = \frac{(1+\mu_2)-2\mu_2C_{12}^2}{1-\mu_2C_{12}^2} = 2-\mathrm{tr}(A^{(1)}A^{-1}). \tag{62}$$

Here we used $\mu_1+\mu_2 = 1$.

We obtain the exact expressions of $\langle K_i\rangle$ for a double pendulum by substituting these into Eq. (47) and expanding $\det A$ as a series of $\mu_2C_{12}^2$.

$$\langle K_1\rangle = \frac{1}{2\beta}\frac{\mu_1\sum_{n=0}^{\infty}\frac{(2n-1)!!}{n!2^n}\mu_2^nR_n(\alpha_1,\alpha_2)}{I_0(\alpha_1)I_0(\alpha_2)-\sum_{n=1}^{\infty}\frac{(2n-3)!!}{n!2^n}\mu_2^nR_n(\alpha_1,\alpha_2)}, \tag{63}$$

$$\langle K_2\rangle = \frac{1}{\beta}-\langle K_1\rangle, \tag{64}$$

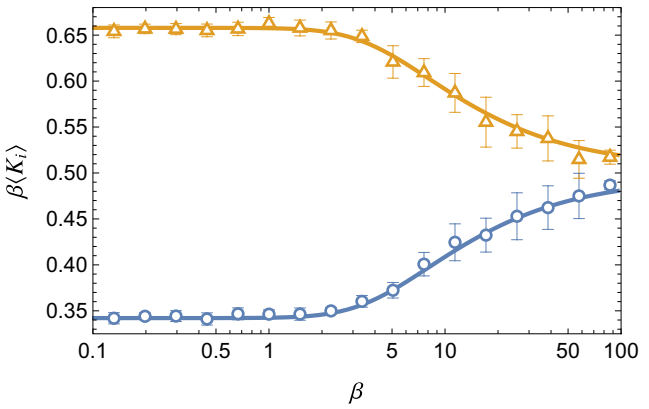

FIG. 10. β dependence of the exact expression of $\langle K_i\rangle$ for double pendulum Eqs. (63) and (64). $\beta\cdot\langle K_i\rangle$ are plotted. The upper and lower curves represent $\langle K_2\rangle$ and $\langle K_1\rangle$, respectively, obtained from Eqs. (64) and (63), respectively. The symbols represent the numerically obtained values of Eq. (36) using the MCMC method. $m_i = 1/2$, $\ell_i = 1$ for $i = 1, 2$; $g = 1$.

where we define $(-1)!! = 1$ and

$$R_n(\alpha_1,\alpha_2) = \sum_{j=0}^{n}\binom{2n}{2j}\{[2(n-j)-1]!!\}^2 \cdot\left\{\frac{\partial^{2j}}{\partial\alpha_1^{2j}}\left[\frac{I_{n-j}(\alpha_1)}{\alpha_1^{n-j}}\right]\right\}\left\{\frac{\partial^{2j}}{\partial\alpha_2^{2j}}\left[\frac{I_{n-j}(\alpha_2)}{\alpha_2^{n-j}}\right]\right\}, \tag{65}$$

$$\alpha_1 = \beta(m_1+m_2)g\ell_1, \tag{66}$$

$$\alpha_2 = \beta m_2g\ell_2, \tag{67}$$

$$\binom{2n}{2j} = \frac{(2n)!}{(2j)!(2n-2j)!}, \tag{68}$$

and $I_n(z)$ is the modified Bessel function of the nth order [29].

Figure 10 shows the values of $\langle K_i\rangle$, $i = 1, 2$, calculated from Eqs. (63) and (64). In addition we show the result of Eq. (36) obtained from MCMC method by symbols to check the validity of Eqs. (63) and (64). We see that both calculations agree quite well.

In this figure, we see that $\beta\cdot\langle K_i\rangle$ appear to converge to certain finite values as $\beta\to 0$. In fact, they are calculated as

$$\lim_{\beta\to0}\beta\cdot\langle K_1\rangle = \frac{\mu_1}{2}\frac{K(\sqrt{\mu_2})}{E(\sqrt{\mu_2})}, \tag{69}$$

and $\lim_{\beta\to0}\beta\cdot\langle K_2\rangle$ is calculated from Eq. (64). Here $K(k)$ and $E(k)$ represent the complete elliptic integrals of the first and second kinds [29], respectively. The derivation of Eq. (69) is presented in Appendix H. From this, we see that the average kinetic energies do not depend on ℓ_i or g at the high-temperature limit.

When $m_1 = m_2$, i.e., $\mu_1 = \mu_2 = 1/2$, we see that

$$\lim_{\beta\to0}\beta\cdot\langle K_1\rangle = 0.3431\ldots, \tag{70}$$

$$\lim_{\beta\to0}\beta\cdot\langle K_2\rangle = 0.6568\ldots. \tag{71}$$

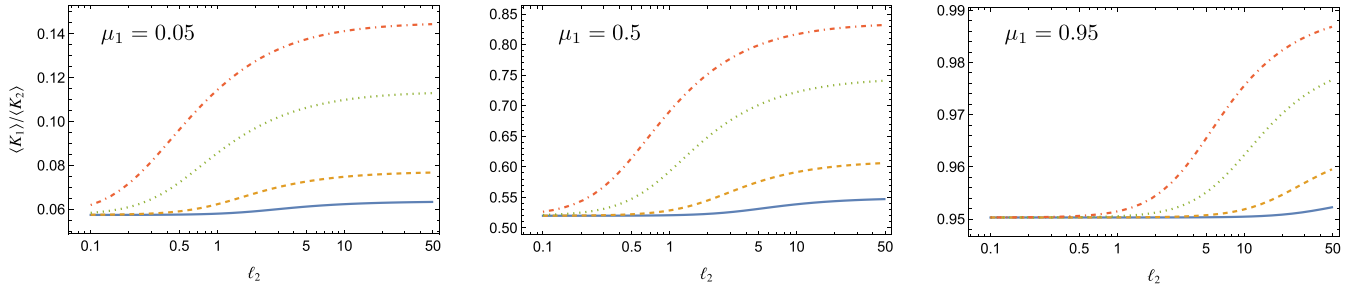

FIG. 11. ℓ_2 dependence of the ratio $\langle K_1\rangle/\langle K_2\rangle$ obtained from the exact expression for double pendulum Eqs. (63) and (64). Values of μ_1 are (left) $\mu_1 = 0.05$, (middle) $\mu_1 = 0.5$, and (right) $\mu_1 = 0.95$. Colors represent $\beta = 1, 2, 5$, and 10 from blue to red. $\ell_1 = 1$.

These values agree well with the values obtained from the MCMC method, as shown in Fig. 10.

Now that we have obtained the exact expression for $\langle K_i\rangle$, we can analyze their dependence on the parameters.

In Fig. 11, we show the ℓ_2 dependence of the ratio $\langle K_1\rangle/\langle K_2\rangle$ for $\mu_1 = 0.05$, 0.5, and 0.95. In every case, as ℓ_2 increases, that is, the length of the lower pendulum increases, the ratio $\langle K_1\rangle/\langle K_2\rangle$ increases.

In Fig. 12, we plot the β dependence of the ratio $\langle K_1\rangle/\langle K_2\rangle$. We see that for $\beta \to 0$, the ratio converges to a positive value, and around $\beta \sim 1$, the ratio increases gradually.

In these figures, we note two remarkable features:

(i) At every temperature we have $\langle K_1\rangle < \langle K_2\rangle$. That is, the particle at the end of the pendulum has a larger average kinetic energy than the other particle near the root.

(ii) The difference between the average kinetic energies is large for high temperatures and small for low temperatures, and a crossover temperature is observed near $\beta = 1$.

The first feature is proved as follows. From Eq. (61) and $\mu_1 + \mu_2 = 1$, we have

$$0 \leqslant \mathrm{tr}(A^{(1)}A^{-1}) \leqslant 1 \leqslant \mathrm{tr}(A^{(2)}A^{-1}) \leqslant 2. \tag{72}$$

From Eqs. (72) and (43) we obtain

$$0 \leqslant \langle K_1\rangle \leqslant \frac{1}{2\beta} \leqslant \langle K_2\rangle \leqslant \frac{1}{\beta} \tag{73}$$

for any values of parameters m_i, ℓ_i, and for any temperature. Hence, the particle at the end always has a larger average kinetic energy than the other particle for a double pendulum.

Let us examine the latter feature. In Fig. 13, we show $\langle\cos\varphi_i\rangle$ calculated by the MCMC method. We observe that for high temperatures $\beta \sim 0$, $\langle\cos\varphi_i\rangle \sim 0$ for both $i = 1$ and $i = 2$. Hence, angles take various values, and the pendulum shows the rotational motion. For low temperature $\beta \gg 1$, $\langle\cos\varphi_i\rangle \sim 1$ that is, $\varphi_i \sim 0$ for both $i = 1$ and $i = 2$; the pendulum exhibits a small-angle liberation. Hence, the crossover temperature observed in Fig. 10 is related to crossover between the librational and rotational motions of the pendulum.

The change in the motion was observed by examining the Poincaré surface of the section of the double pendulum. Figure 14 shows the Poincaré surface of section (φ_2, p_2) taken at $\varphi_1 = 0$ and $p_1 - p_2\cos\varphi_2 > 0$ for several values of the total energy. The definition of the section is explained in Appendix I. As the total energy E approaches $E \sim 1$, the chaotic region in the phase space rapidly expands and fills most of the energy surface. Moreover, the energy surface itself expands rapidly around $E \sim 1$. Hence, we interpret the crossover near $\beta \sim 1$ found in Figs. 11 and 12 as the change in the energy surface.

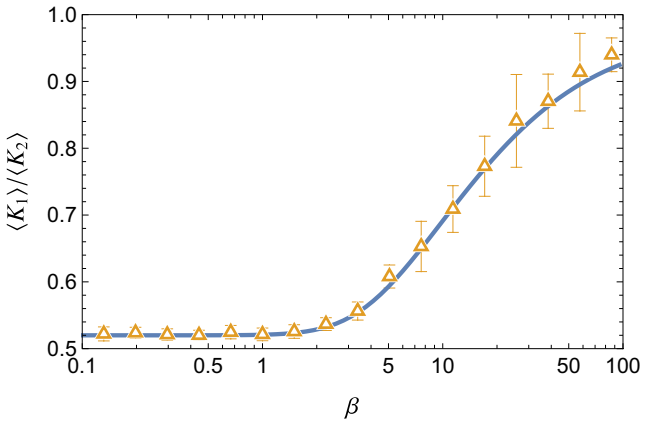

FIG. 12. β dependence of the ratio $\langle K_1\rangle/\langle K_2\rangle$ of a double pendulum. The solid line represents the values obtained from the exact expressions Eqs. (63) and (64), and the symbols represent values obtained by the MCMC method.

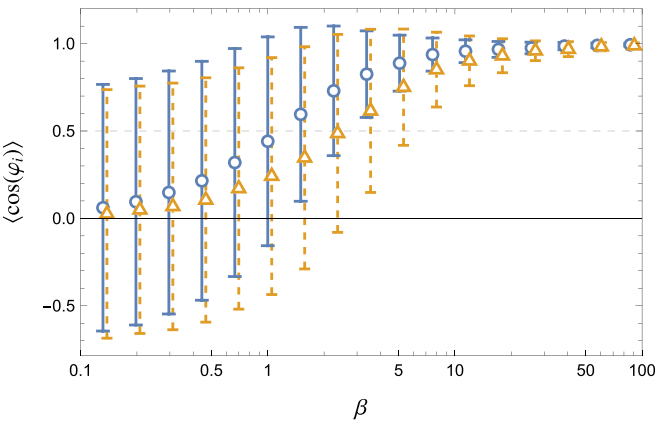

FIG. 13. β dependence of $\langle\cos(\varphi_i)\rangle$ obtained by the MCMC method. Open circles represent $i = 1$, and open triangles represent $i = 2$. The parameters were the same as those in Fig. 10.

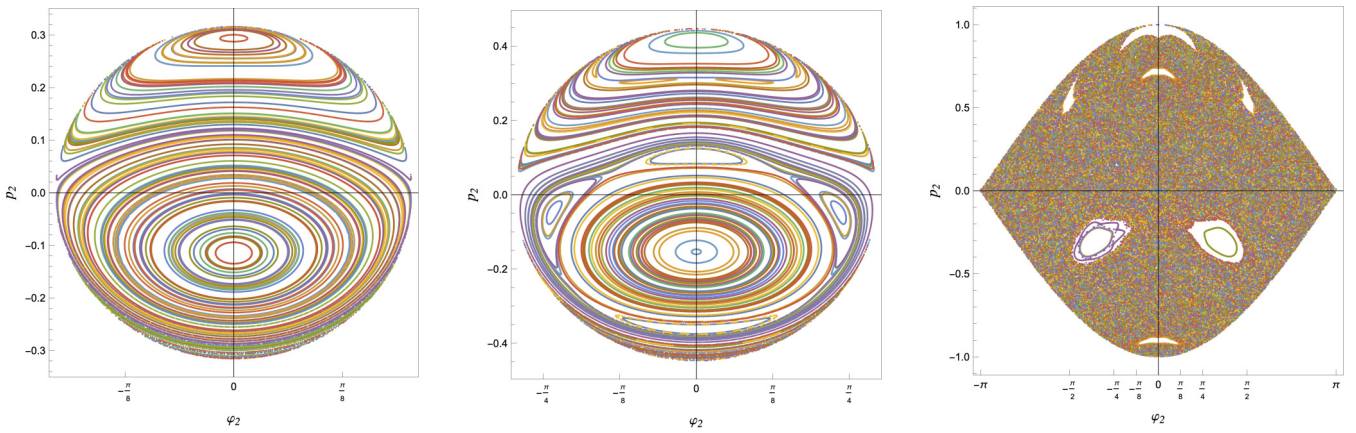

FIG. 14. Poincaré surface of section (φ_2, p_2) at $\varphi_1 = 0$, $p_1 - p_2 \cos\varphi_2 > 0$. The definition of this section is explained in the Appendix I. $m_1 = m_2 = 1$, and $\ell_1 = \ell_2 = 1$. The values of the total energy are (left) $E = 0.1$, (middle) $E = 0.2$, and (right) $E = 1.0$. Here we take the origin of the potential energy at $y_1 = -\ell_1$ and $y_2 = -(\ell_1 + \ell_2)$, i.e., when the pendulum is at the lowermost place.

V. SUMMARY AND DISCUSSIONS

We showed that the averages of the kinetic energies of particles in multiple pendulum take different values via numerical computation and analytical calculations. Since the multiple pendulum has holonomic constraints, uniformity of average kinetic energy of each particle at thermal equilibrium is no longer guaranteed. On the contrary, another quantity what we call canonical kinetic energy is uniform, and the uniformity is guaranteed by the generalized principle of equipartition of energy. Moreover, the uniformity of the average canonical kinetic energy yields nonuniformity of the average kinetic energy of each particle.

Systems with holonomic constraints do not obey the (conventional) principle of the equipartition of energy, but a generalized one. Our discovery added a new example in which we can see how the system systematically deviates from (not generalized) equipartition [24,30].

Each particle's average kinetic energy does not take the same value because it is not the quantity whose uniformity is guaranteed by the generalized principle of equipartition of energy. The difference comes from the fact that the kinetic energy depends on coordinates; this dependence is attributed to the existence of holonomic constraints. In short, the holonomic constraints give rise to the nonuniform distribution of the average linear kinetic energies. This scenario is similar to a chain system without a fixed root, i.e., a freely jointed chain. Freely jointed chain is a simplified model of polymers and is composed of particles connected by massless rigid links [31–40]. For a freely jointed chain composed of identical masses, the average kinetic energy of each particle is large near both ends of the chain and small near the middle of the chain [24,30].

For a double pendulum, we successfully obtained the exact expressions for the thermal average of kinetic energy of each particle $\langle K_i \rangle$. They include temperature, mass of two particles, lengths of two links, and constant of gravitational acceleration. Hence, the exact expression is useful to design a system that has predefined values of average kinetic energy. Exact expressions for average kinetic energies are also obtained for a three-particle two-dimensional freely jointed chain [30], where nonuniformity of the average kinetic energies is also shown.

Further, we showed that the dependence of $\beta \cdot \langle K_i \rangle$ on the mass and length of links vanish in the high-temperature limit. The reason why $\beta \cdot \langle K_i \rangle$ does not depend on ℓ_i or g is interpreted as follows: $\langle K_i \rangle$ depends on ℓ_i or g only through coupling with β, as in Eq. (66) and (67). Hence, in the limit $\beta \to 0$, the dependence on ℓ_i or g vanishes. Incidentally, this independence is also seen in the approximate expression in Eq. (50), although the approximation is not derived from high-temperature limit.

In this paper we studied the effect of holonomic constraint on the equipartition property. There are other systems which have nonholonomic constraints. For example, constraints represented by coordinates and momenta, and constraints represented by inequalities. The former one is realized by the existence of conserved quantities [41,42]. The latter is also an interesting subject of future research.

We considered a multiple pendulum which have holonomic constraints, and the holonomic constraints are essential for nonuniformity of average kinetic energies for the system. In real systems there are no exact holonomic constraints; constraints appearing in models are often approximations of stiff springs and hard potentials. Suppose we have a multiple spring-pendulum where the rigid links in the multiple pendulum are replaced by springs. If the potentials are sufficiently hard, then there will be a large gap between timescales of swinging motion of pendulum and vibrational motion of springs. Then, according to Boltzmann-Jeans theory [43–51], the energy exchange between swinging motion of pendulum and vibrational motion of springs take quite long time, typically exponentially long with respect to the spring constant. Then we have a good chance to observe the system well approximated by rigid multiple pendulum, and average kinetic energies are nonuniform for quite long time.

ACKNOWLEDGMENTS

We thank Mikito Toda and Yoshiyuki Y. Yamaguchi for their fruitful discussions. T.K. was supported by a

Chubu University Grant (A). T.Y. acknowledges the support of the Japan Society for the Promotion of Science (JSPS) KAKENHI Grants No. 18K03471 and No. 21K03411. We thank anonymous reviewers for their fruitful comments.

APPENDIX A: DERIVATION OF THE LAGRANGIAN AND HAMILTONIAN OF A MULTIPLE PENDULUM

Here we show a detailed derivation of the Lagrangian of a multiple pendulum [Eq. (4)]. To obtain a canonical momentum conjugate to the angle φ_i,

$$p_i = \frac{\partial L}{\partial \dot{\varphi}_i}, \tag{A1}$$

we need to express L (i.e., the kinetic energy T) in terms of φ_i and $\dot{\varphi}_i$.

First, we consider that the angles φ and Cartesian coordinates x, y are related as

$$x_i = x_{i-1} + \ell_i \sin\varphi_i = \sum_{j=1}^{i} \ell_j \sin\varphi_j, \tag{A2}$$

$$y_i = y_{i-1} - \ell_i \cos\varphi_i = -\sum_{j=1}^{i} \ell_j \cos\varphi_j. \tag{A3}$$

Then, we have

$$\begin{aligned}\dot{x}_i^2 + \dot{y}_i^2 &= \left(\sum_{j=1}^{i} \ell_j \dot{\varphi}_j \cos\varphi_j\right)^2 + \left(\sum_{j=1}^{i} \ell_j \dot{\varphi}_j \sin\varphi_j\right)^2 \\ &= \sum_{j=1}^{i}\sum_{k=1}^{i} \ell_j \ell_k \dot{\varphi}_j \dot{\varphi}_k (\cos\varphi_j \cos\varphi_k + \sin\varphi_j \sin\varphi_k) \\ &= \sum_{j=1}^{i}\sum_{k=1}^{i} \ell_j \ell_k \dot{\varphi}_j \dot{\varphi}_k \cos(\varphi_j - \varphi_k)\end{aligned} \tag{A4}$$

and the kinetic energy K reads

$$K = \sum_{i=1}^{N} \frac{m_i}{2} \sum_{j=1}^{i}\sum_{k=1}^{i} \ell_j \ell_k \dot{\varphi}_j \dot{\varphi}_k \cos(\varphi_j - \varphi_k). \tag{A5}$$

Using an identity

$$\sum_{i=1}^{N}\sum_{j=1}^{i}\sum_{k=1}^{i} = \sum_{j=1}^{N}\sum_{k=1}^{N}\left[\sum_{i=\max(j,k)}^{N}\right], \tag{A6}$$

we obtain

$$K = \frac{1}{2}\sum_{j=1}^{N}\sum_{k=1}^{N}\left[\sum_{i=\max(j,k)}^{N} m_i\right] \ell_j \ell_k \dot{\varphi}_j \dot{\varphi}_k \cos(\varphi_j - \varphi_k), \tag{A7}$$

$$= \frac{1}{2}\sum_{j=1}^{N}\sum_{k=1}^{N} A_{jk}(\varphi)\dot{\varphi}_j\dot{\varphi}_k = \frac{1}{2}{}^t\dot{\varphi} A \dot{\varphi}, \tag{A8}$$

where the elements of $N \times N$ matrix $A(\varphi)$ is defined as

$$A_{jk}(\varphi) = \left[\sum_{i=\max(j,k)}^{N} m_i\right] \ell_j \ell_k \cos(\varphi_j - \varphi_k), \tag{A9}$$

and $\dot{\varphi}$ without subscript is

$$\dot{\varphi} = {}^t(\dot{\varphi}_1, \ldots, \dot{\varphi}_N). \tag{A10}$$

Using Eq. (A8), the Lagrangian of the multiple pendulum is expressed in terms of the angles φ and $\dot{\varphi}$ as

$$\begin{aligned}L &= \frac{1}{2}\sum_{j=1}^{N}\sum_{k=1}^{N} A_{jk}(\varphi)\dot{\varphi}_j\dot{\varphi}_k + \sum_{i=1}^{N} m_i g \sum_{j=1}^{i} \ell_j \cos\varphi_j \\ &= \frac{1}{2}{}^t\dot{\varphi} A \dot{\varphi} + \sum_{i=1}^{N} m_i g \sum_{j=1}^{i} \ell_j \cos\varphi_j,\end{aligned} \tag{A11}$$

The canonical momentum p_n conjugate to the angle φ_n ($n = 1, 2, \ldots, N$) can be obtained using the expression of the Lagrangian [Eq. (A11)] as

$$p_n = \frac{\partial L}{\partial \dot{\varphi}_n} = \sum_{k=1}^{N} A(\varphi)_{nk}\dot{\varphi}_k = [A(\varphi)p]_n, \tag{A12}$$

$$K = \sum_{i,j=1}^{N} \frac{1}{2} A(\varphi)_{ij}\dot{\varphi}_i\dot{\varphi}_j = \frac{1}{2}{}^t\dot{\varphi} A(\varphi)\,\dot{\varphi} \tag{A13}$$

$$= \sum_{i,j=1}^{N} \frac{1}{2}[A^{-1}(\varphi)]_{ij} p_i p_j \tag{A14}$$

$$= \frac{1}{2}{}^t p A^{-1}(\varphi) p. \tag{A15}$$

Here p without subscript is

$$p = {}^t(p_1, \ldots, p_N). \tag{A16}$$

Then the Hamiltonian of the multiple pendulum is obtained by the standard procedure as

$$\begin{aligned}H &= \sum_{i=1}^{n} p_i\dot{\varphi}_i - L \\ &= \sum_{i,j=1}^{N} \frac{1}{2}[A^{-1}(\varphi)]_{ij} p_i p_j + U(\varphi),\end{aligned} \tag{A17}$$

$$= \frac{1}{2}{}^t p A^{-1}(\varphi) p + U(\varphi). \tag{A18}$$

APPENDIX B: NUMERICAL METHOD OF THE LYAPUNOV EXPONENTS FOR MULTIPLE PENDULUMS

The Hamiltonian of a multiple pendulum is given in Eq. (21). The difficulty of the numerical integration comes from the computational cost of the inverse matrix A^{-1}. In principle we can obtain analytic expression for A^{-1} but it consists of huge number of terms. To simulate the multiple pendulums, we estimate the inverse matrix A^{-1} numerically from the analytic expression of A for given φ_i [Eq. (12)]. The Hamilton equations,

$$\frac{\partial \varphi_i}{\partial t} = \frac{\partial H}{\partial p_i} = \sum_k A^{-1}_{i,k}\, p_k, \tag{B1}$$

$$\frac{\partial p_i}{\partial t} = -\frac{\partial H}{\partial \varphi_i} = \frac{1}{2} p^t \left(A^{-1}\frac{\partial A}{\partial \varphi_i} A^{-1}\right) p - \frac{\partial V}{\partial \varphi_i}, \tag{B2}$$

are integrated using the inverse matrix A^{-1} by an implicit Runge-Kutta method called "Gauss method," which is known to be symplectic [52]. To calculate the Lyapunov exponents [53], the Jacobian of the Hamilton equations is calculated using the numerically obtained A^{-1} as follows:

$$J = \begin{pmatrix} J_1 & J_2 \\ J_3 & J_4 \end{pmatrix}, \tag{B3}$$

where J_1, J_2, J_3, and J_4 are $(N \times N)$ matrices, and the elements of those are given by

$$(J_1)_{ij} = \frac{\partial \dot{\varphi}_i}{\partial \varphi_j} \tag{B4}$$

$$= \frac{\partial}{\partial \varphi_j} \sum_k^N A^{-1}_{ik} p_k \tag{B5}$$

$$= -\sum_k^N \left(A^{-1} \frac{\partial A}{\partial \varphi_j} A^{-1} \right)_{ik} \cdot p_k, \tag{B6}$$

$$(J_2)_{ij} = \frac{\partial \dot{\varphi}_i}{\partial p_j} \tag{B7}$$

$$= \frac{\partial}{\partial p_j} \sum_k^N A^{-1}_{ik} p_k \tag{B8}$$

$$= A^{-1}_{ij}, \tag{B9}$$

$$(J_3)_{ij} = \frac{\partial \dot{p}_i}{\partial \varphi_j} \tag{B10}$$

$$= \frac{1}{2} p^t \left[-A^{-1} \left\{ \frac{\partial A}{\partial \varphi_j} A^{-1} \frac{\partial A}{\partial \varphi_i} - \frac{\partial^2 A}{\partial \varphi_j \partial \varphi_i} + \frac{\partial A}{\partial \varphi_i} A^{-1} \frac{\partial A}{\partial \varphi_j} \right\} A^{-1} \right] p - \frac{\partial^2 V}{\partial \varphi_i \partial \varphi_j}, \tag{B11}$$

$$(J_4)_{ij} = \frac{\partial \dot{p}_i}{\partial p_j} \tag{B12}$$

$$= \sum_k^N \left(A^{-1} \frac{\partial A}{\partial \varphi_i} A^{-1} \right)_{jk} p_k, \tag{B13}$$

respectively. Along an orbit $(q(t_\ell), p(t_\ell))$ where $t_\ell = \delta t \cdot \ell$ $(\ell = 0, 1, \ldots, L)$ obtained by solving the Hamilton equations every δt, the Jacobian $J(q(t_\ell), p(t_\ell))$ can be calculated. The time evolution of tangent vector ξ is governed by

$$\frac{d\xi}{dt} = J(q(t), p(t))\xi, \tag{B14}$$

and we solve $2N$ number of tangent vectors ξ^i $(i = 1, 2, \ldots, 2N)$ simultaneously by the Euler method as follows:

$$\xi^i(t_{\ell+1}) = \{I_{2N} + \delta t J(q(t_\ell), p(t_\ell))\}\xi^i(t_\ell) \tag{B15}$$

$$(i = 1, 2, \ldots, 2N), \tag{B16}$$

where I_{2N} is the $(2N \times 2N)$ identity matrix. To estimate the local expansion rates of nearby trajectories, we use the Gram-Schmidt orthogonalization method every m steps [54], and the expansion rates are given by

$$\eta_i(t_{m\ell}) = \frac{||\tilde{\xi}^i(t_{m\ell})||}{||\xi^i(t_{m\ell})||}, \quad (i = 1, 2, \ldots, N), \quad (\ell = 1, 2, \ldots L), \tag{B17}$$

where $\tilde{\xi}^i(t_{m\ell})$ is the tangent vectors after the orthogonalization. Finally, the Lyapunov exponents are estimated by

$$\lambda_i = \frac{\sum_{\ell=1}^L \log(\eta_i(t_{m\ell}))}{m L \delta t}. \tag{B18}$$

In Fig. 5, the initial time series $t < 100$ were discarded. We use the following parameters: $\delta t = 0.001$, $m = 100$, and $m L \delta t = 1000$.

APPENDIX C: "CANONICAL KINETIC ENERGY"

Our Hamiltonian has the form

$$H = \sum_{ij} \frac{1}{2} (A^{-1})_{ij}(q) p_i p_j + V(q), \tag{C1}$$

where q and p are generalized coordinates and their conjugate momenta, respectively.

The generalized principle of the equipartition of energy is expressed as

$$\left\langle \frac{1}{2} p_i \frac{\partial H}{\partial p_i} \right\rangle = \frac{1}{2} k_B T \quad \text{(no sum for } i\text{)}. \tag{C2}$$

Here k_B denotes Boltzmann's constant and T represents the temperature, respectively.

$K_i^{(c)}$ is defined as

$$K_i^{(c)} = \frac{1}{2} p_i \frac{\partial H}{\partial p_i} \quad \text{(no sum for } i\text{)}. \tag{C3}$$

$K_i^{(c)}$ is not always the same as the traditional kinetic energy of the ith degrees of freedom,

$$K_i = \tfrac{1}{2} m_i \dot{q}_i^2 \quad \text{(no sum for } i\text{)}, \tag{C4}$$

because of the off-diagonal terms in the quadratic form. To clarify this distinction, we call $K_i^{(c)}$ the "canonical kinetic energy" and K_i the "linear kinetic energy" in this paper [55].

Below, we compute the "canonical kinetic energy" of the general multiple pendulum.

Our Hamiltonian is of the form

$$H(q, p) = K(q, p) + V(q) \tag{C5}$$

and we have for "canonical kinetic energy,"

$$K_i^{(c)} = \frac{1}{2} p_i \frac{\partial H}{\partial p_i} = \frac{1}{2} p_i \frac{\partial K}{\partial p_i} \quad \text{(no sum for } i\text{)} \tag{C6}$$

$$= \frac{1}{2} p_i \frac{\partial}{\partial p_i} \sum_{j,k=1}^N \frac{1}{2} (A^{-1})_{jk} p_j p_k \quad \text{[from (A15)]} \tag{C7}$$

$$= \sum_{k=1}^N \frac{1}{2} p_i (A^{-1})_{ik} p_k = \frac{1}{2} p_i \dot{\varphi}_i \quad \text{(no sum for } i\text{)}. \tag{C8}$$

The sum of the "canonical kinetic energy" of the ith angle $K_i^{(c)}$ is equal to the (total) kinetic energy K, which is given as

$$K = \sum_{i=1}^{N}\left[\frac{1}{2}p_i\sum_{k=1}^{N}(A^{-1})_{ik}p_k\right] = \sum_{i=1}^{N}K_i^{(c)}. \tag{C9}$$

Now, we express $K_i^{(c)}$ in terms of φ and $\dot{\varphi}$, and then in terms of the Cartesian coordinate x, y. Since $K = \frac{1}{2}{}^t pA^{-1}p$, we have $\frac{\partial K}{\partial p_i} = (A^{-1}p)_i = \dot{\varphi}_i$. Hence, $K_i^{(c)}$ is expressed as

$$K_i^{(c)} = \frac{1}{2}p_i\frac{\partial H}{\partial p_i}(\text{no sum for } i) \tag{C10}$$

$$= \frac{1}{2}p_i\dot{\varphi}_i \tag{C11}$$

$$= \sum_{j=1}^{N}\frac{1}{2}A_{ij}\dot{\varphi}_j\dot{\varphi}_i \tag{C12}$$

$$= \sum_{j=1}^{N}\frac{1}{2}\left[\sum_{n=\max(i,j)}^{N}m_n\right]\ell_i\ell_j\cos(\varphi_i-\varphi_j)\dot{\varphi}_j\dot{\varphi}_i. \tag{C13}$$

This is the formula which represents "canonical kinetic energy" of the ith degree of freedom in terms of φ and $\dot{\varphi}$.

Let us express $K_i^{(c)}$ in terms of Cartesian coordinates x_j and y_j. The result is

$$K_i^{(c)} = \frac{1}{2}(\dot{x}_i-\dot{x}_{i-1})\left(\sum_{j=i}^{N}m_j\dot{x}_j\right) + \frac{1}{2}(\dot{y}_i-\dot{y}_{i-1})\left(\sum_{j=i}^{N}m_j\dot{y}_j\right). \tag{C14}$$

As expected, this expression for "canonical kinetic energy" $K_i^{(c)}$ is different from the "linear" kinetic energy $K_i = \frac{1}{2}m_i(\dot{x}_i^2+\dot{y}_i^2)$. Although $K_i^{(c)}$ is defined from the momentum p_i, which is canonically conjugate to the (local) angle φ_i, $K_i^{(c)}$ depends on the coordinates of all the particles $j = 1, 2, \ldots, N$ and extended over the entire system, whereas K_i is localized to a particular particle i.

1. Example: Double pendulum

Setting $N = 2$ in Eq. (C14), we have the following expressions for the "canonical kinetic energy" of a double pendulum:

$$K_1^{(c)} = \tfrac{1}{2}\{m_1(\dot{x}_1^2+\dot{y}_1^2)+m_2(\dot{x}_1\dot{x}_2+\dot{y}_1\dot{y}_2)\}, \tag{C15}$$

$$K_2^{(c)} = \tfrac{1}{2}m_2\{(\dot{x}_2^2+\dot{y}_2^2)-(\dot{x}_1\dot{x}_2+\dot{y}_1\dot{y}_2)\}. \tag{C16}$$

We see that

$$K_1^{(c)} \neq K_1 = \tfrac{1}{2}m_1(\dot{x}_1^2+\dot{y}_1^2), \tag{C17}$$

$$K_2^{(c)} \neq K_2 = \tfrac{1}{2}m_2(\dot{x}_2^2+\dot{y}_2^2), \tag{C18}$$

$$K_1^{(c)} + K_2^{(c)} = K_1 + K_2. \tag{C19}$$

Therefore, at thermal equilibrium, we have the average kinetic energy of each particle of a double pendulum, which is not equal to $\frac{1}{2}k_BT$;

$$\langle K_i\rangle \neq \tfrac{1}{2}k_BT, \quad i = 1, 2, \tag{C20}$$

$$\langle K_1\rangle \neq \langle K_2\rangle. \tag{C21}$$

APPENDIX D: GENERALIZED PRINCIPLE OF THE EQUIPARTITION OF ENERGY

Assume that we have a Hamiltonian of the form:

$$H = K(q, p) + U(q), \tag{D1}$$

where $K(q, p)$ and $U(q)$ are the kinetic and potential energies, respectively. Here $K(q, p)$ depends on coordinate q. The "generalized principle of equipartition of energy" states that, if a system whose Hamiltonian is in the form of Eq. (D1) is in thermal equilibrium at temperature T, then

$$\left\langle\frac{1}{2}p_i\frac{\partial H}{\partial p_i}\right\rangle = \frac{1}{2}k_BT \tag{D2}$$

holds for each degree of freedom i. Here p_i represents the canonical momenta, and summation is not taken for repeated index i.

Proof of this principle is similar to that of the conventional case. The thermal average of an arbitrary quantity $f(q, p)$ is defined as

$$\langle f(q,p)\rangle = \frac{1}{\mathcal{Z}}\int f(q,p)e^{-\beta H}d^Np\,d^Nq, \tag{D3}$$

where $\mathcal{Z}$ is the partition function

$$\mathcal{Z} = \int e^{-\beta H}d^Np\,d^Nq. \tag{D4}$$

Since

$$\frac{\partial}{\partial p_i}e^{-\beta H} = e^{-\beta H}(-\beta)\frac{\partial H}{\partial p_i}, \tag{D5}$$

we have

$$\frac{\partial H}{\partial p_i}e^{-\beta H} = -\frac{1}{\beta}\frac{\partial}{\partial p_i}e^{-\beta H}. \tag{D6}$$

Hence

$$\int p_i\frac{\partial H}{\partial p_i}e^{-\beta H}d^Np = -\frac{1}{\beta}\int p_i\frac{\partial}{\partial p_i}e^{-\beta H}d^Np. \tag{D7}$$

In the N-fold integration let us perform first the integral with respect to p_i:

$$\int p_i\frac{\partial}{\partial p_i}e^{-\beta H}d^Np = \int\cdots\int\left(\int p_i\frac{\partial}{\partial p_i}e^{-\beta H}dp_i\right)d^{N-1}p. \tag{D8}$$

Using integration by parts we have

$$\int p_i\frac{\partial}{\partial p_i}e^{-\beta H}dp_i = [p_ie^{-\beta H}]_{p_i=-\infty}^{p_i=+\infty} - \int e^{-\beta H}dp_i. \tag{D9}$$

Let us assume that

$$\lim_{p_i\to\pm\infty}p_ie^{-\beta H} = 0. \tag{D10}$$

This assumption is satisfied when $H = K(q, p) + U(q)$ and $K(q, p) = \frac{1}{2}{}^t pA^{-1}(q)p$, where A^{-1} is an $N \times N$ positive definite matrix.

Then

$$\int p_i \frac{\partial}{\partial p_i} e^{-\beta H} d^N p = \int \cdots \int \left(- \int e^{-\beta H} dp_i \right) d^{N-1} p = - \int e^{-\beta H} d^N p. \tag{D11}$$

Hence we have

$$\int p_i \frac{\partial H}{\partial p_i} d^N p = \frac{1}{\beta} \int e^{-\beta H} d^N p, \tag{D12}$$

and Eq. (D2), that is, the generalized principle of equipartition of energy holds.

The generalized principle of equipartition includes conventional principle of equipartition. If the Hamiltonian is of the form

$$H(q, p) = K(p) + U(q), \tag{D13}$$

$$K(p) = \sum_i \frac{1}{2m_i} p_i^2, \tag{D14}$$

then

$$\frac{1}{2} p_i \frac{\partial H}{\partial p_i} = \frac{1}{2m_i} p_i^2 \tag{D15}$$

and Eq. (D2) implies

$$\left\langle \frac{1}{2m_i} p_i^2 \right\rangle = \frac{1}{2} k_B T, \tag{D16}$$

that is, conventional equipartition holds.

APPENDIX E: METHOD OF MCMC SIMULATION

For MCMC simulations, we use the Metropolis algorithm [56,57]. The variables in the Hamiltonian are general coordinates and their conjugate momenta, as shown in Eq. (21). To estimate A^{-1} in the Hamiltonian, we compute the inverse matrix A^{-1} numerically from the analytic expression of A for given φ_i [Eq. (12)]. Then, the state of MCMC for the Hamiltonian is $\vec{s} = (\varphi_1, \varphi_2, \ldots, \varphi_N, p_1, p_2, \ldots p_N)$, and the initial value of $\vec{s}$ is set to $\vec{s}^{\,(0)}$, where all elements of $\vec{s}^{\,(0)}$ are drawn from the normal distribution, i.e., $f(x) \sim \exp\{-\frac{1}{2}[(x - \mu)/\sigma]^2\}$, where μ is the mean and σ is the standard deviation, respectively. The iteration of the algorithm is described as follows:

(i) Choose a perturbation to current states $\vec{\delta s}$ as all elements are drawn from the normal distribution $f(x)$, When the current value of $\vec{s}$ is $\vec{s}^{\,(n)}$, the candidate of next state is defined by $\vec{s}^{\,\prime} = \vec{s}^{\,(n)} + \vec{\delta s}$

(ii) Draw a uniform random number $R \in [0, 1)$. If and only if

$$R < \frac{\exp[-\beta H(\vec{s}^{\,\prime})]}{\exp[-\beta H(\vec{s}^{\,(n)})]},$$

the candidate is accepted: $\vec{s}^{\,(n+1)} = \vec{s}^{\,\prime}$; otherwise, nothing is changed: $\vec{s}^{\,(n+1)} = \vec{s}^{\,(n)}$

(iii) Return to step (i).

After initial m_0 transient steps, we calculate the kinetic energy of i-th particle $K_i(\vec{s}^{\,(m)})$ for every k steps, where $m = m_0 + k(j - 1)$, $(j = 1, 2, \ldots, M)$. Then, the estimated value of the kinetic energy is obtained by average over these M samples. The statistical error is calculated by K different runs. The parameters used in Fig. 7 are $m_0 = 10\,000$, $k = 10$, $M = 1000$, $K = 100$, and $\sigma = 0.25/\sqrt{N\beta}$, respectively. β in Eq. (36) is defined as follows. Given a total kinetic energy $\sum_{i=1}^N \overline{K_i}$, the value of β used in Fig. 7 for $\langle K_i \rangle$ is implicitly determined from the following equation:

$$\sum_{i=1}^N \langle K_i \rangle = \sum_{i=1}^N \overline{K_i}. \tag{E1}$$

APPENDIX F: DERIVATION OF EQ. (43) $\langle K_i \rangle = \frac{1}{2\beta} \langle \mathrm{tr}(A^{(i)} A^{-1}) \rangle$

Here we derive the expression for average kinetic energy, Eq. (43), that is,

$$\langle K_i \rangle = \frac{1}{2\beta} \langle \mathrm{tr}(A^{(i)} A^{-1}) \rangle. \tag{F1}$$

From Eq. (20) the average $\langle K_i \rangle$ reads

$$\langle K_i \rangle = \frac{1}{Z} \int \frac{1}{2} \sum_{j,k,\xi,\eta} A^{(i)}_{jk} A^{-1}_{j\xi} A^{-1}_{k\eta} p_\xi p_\eta e^{-\beta H} d\Gamma. \tag{F2}$$

Using

$$\frac{\partial}{\partial p_k} e^{-\beta H} = -\beta \sum_{\eta=1}^N A^{-1}_{k\eta} p_\eta e^{-\beta H}, \tag{F3}$$

we have

$$\sum_{\eta=1}^N A^{-1}_{k\eta} p_\eta e^{-\beta H} = \frac{-1}{\beta} \frac{\partial}{\partial p_k} e^{-\beta H}. \tag{F4}$$

By integrating by parts, we obtain

$$\begin{aligned} &\int \sum_{\eta=1}^N A^{-1}_{k\eta} p_\xi p_\eta e^{-\beta H} d^N p \\ &= \int \frac{-1}{\beta} p_\xi \frac{\partial}{\partial p_k} e^{-\beta H} d^N p \\ &= \int \frac{-1}{\beta} p_\xi [e^{-\beta H}]_{p_k=-\infty}^{p_k=\infty} d^{N-1} p \\ &\quad + \frac{1}{\beta} \int \left(\frac{\partial}{\partial p_k} p_\xi \right) e^{-\beta H} d^N p \\ &= \frac{1}{\beta} \int \delta_{k,\xi} e^{-\beta H} d^N p. \end{aligned} \tag{F5}$$

Therefore

$$\begin{aligned} &\int \frac{1}{2} \sum_{j,k,\xi,\eta} A^{(i)}_{jk} A^{-1}_{j\xi} A^{-1}_{k\eta} p_\xi p_\eta e^{-\beta H} d^N p \\ &= \frac{1}{2} \frac{1}{\beta} \int \sum_{j,k,\xi} A^{(i)}_{jk} A^{-1}_{j\xi} \delta_{k,\xi} e^{-\beta H} d^N p \end{aligned}$$

$$= \frac{1}{2\beta}\int \sum_{j,k} A^{(i)}_{jk} A^{-1}_{jk} e^{-\beta H} d^N p$$
$$= \frac{1}{2\beta}\int \mathrm{tr}(A^{(i)}A^{-1}) e^{-\beta H} d^N p \tag{F6}$$

hence Eq. (43) holds.

APPENDIX G: DERIVATION OF APPROXIMATE EXPRESSION OF $\langle K_i \rangle$ FOR MULTIPLE PENDULUM

Let us start with Eq. (41). By applying the approximation Eq. (48), we have

$$\langle K_i \rangle \approx \frac{m_i}{2} \sum_{j=1}^{i} \ell_j^2 \langle \dot{\varphi}_j^2 \rangle. \tag{G1}$$

Now, let us evaluate $\langle \dot{\varphi}_j^2 \rangle$. Note that

$$\dot{\varphi}_j = \sum_{n=1}^{N} A^{-1}_{jn} p_n = \frac{\partial}{\partial p_j} \frac{1}{2} \sum_{i,n} p_i A^{-1}_{in} p_n = \frac{\partial}{\partial p_j} H. \tag{G2}$$

On the other hand,

$$\frac{\partial}{\partial p_j} e^{-\beta H} = -\beta \frac{\partial H}{\partial p_j} e^{-\beta H}. \tag{G3}$$

Therefore,

$$\dot{\varphi}_j^2 = \left(\sum_{n=1}^{N} A^{-1}_{jn} p_n \right)^2 = \left(\sum_{n=1}^{N} A^{-1}_{jn} p_n \right) \left(\sum_{n=1}^{N} A^{-1}_{jn} p_n \right) \tag{G4}$$
$$= \left(\sum_{n=1}^{N} A^{-1}_{jn} p_n \right) \frac{\partial H}{\partial p_j}, \tag{G5}$$

and

$$\dot{\varphi}_j^2 e^{-\beta H} = \left(\sum_{n=1}^{N} A^{-1}_{jn} p_n \right) \frac{\partial H}{\partial p_j} e^{-\beta H} \tag{G6}$$
$$= \left(\sum_{n=1}^{N} A^{-1}_{jn} p_n \right) \left(\frac{-1}{\beta} \right) \frac{\partial}{\partial p_j} e^{-\beta H}, \tag{G7}$$
$$\int \dot{\varphi}_j^2 e^{-\beta H} d\Gamma = \left(\frac{-1}{\beta} \right) \int \left(\sum_{n=1}^{N} A^{-1}_{jn} p_n \right) \frac{\partial}{\partial p_j} e^{-\beta H} d\Gamma. \tag{G8}$$

Performing integration by parts with respect to p_j, we obtain

$$\int \left(\sum_{n=1}^{N} A^{-1}_{jn} p_n \right) \frac{\partial}{\partial p_j} e^{-\beta H} dp_j \tag{G9}$$
$$= -\int A^{-1}_{jj}(\varphi) \cdot e^{-\beta H} dp_j, \tag{G10}$$

where the summation over j is not taken.

Thus, we have

$$\int \dot{\varphi}_j^2 e^{-\beta H} d\Gamma = \left(\frac{1}{\beta} \right) \int A^{-1}_{jj}(\varphi) e^{-\beta H} d\Gamma, \tag{G11}$$

$$\langle \dot{\varphi}_j^2 \rangle = \frac{1}{\beta} \langle A^{-1}_{jj}(\varphi) \rangle. \tag{G12}$$

Let us evaluate $\langle A^{-1}_{jj}(\varphi) \rangle$. From Eq. (A9), we have

$$A_{jj}(\varphi) = \left(\sum_{i=j}^{N} m_i \right) \ell_j^2. \tag{G13}$$

Let us adopt the approximation Eq. (49)

$$A^{-1}_{jj} \approx \frac{1}{A_{jj}} \tag{G14}$$
$$= \frac{1}{\left(\sum_{i=j}^{N} m_i \right) \ell_j^2}. \tag{G15}$$

This approximation implies that we omit all off-diagonal elements of matrix A, which include phase factors such as $\cos(\varphi_{jk})$.

Then, we have

$$\langle \dot{\varphi}_j^2 \rangle = \frac{1}{\beta} \langle A^{-1}_{jj}(\varphi) \rangle \approx \frac{1}{\beta} \left\langle \frac{1}{\left(\sum_{i=j}^{N} m_i \right) \ell_j^2} \right\rangle \tag{G16}$$
$$= \frac{1}{\beta \left(\sum_{i=j}^{N} m_i \right) \ell_j^2}. \tag{G17}$$

Therefore, we obtain

$$\langle K_i \rangle = \frac{m_i}{2} \langle \dot{x}_i^2 + \dot{y}_i^2 \rangle \approx \frac{m_i}{2} \sum_{j=1}^{i} \langle \dot{\varphi}_j^2 \rangle \ell_j^2 \tag{G18}$$
$$= k_B T \cdot \frac{m_i}{2} \sum_{j=1}^{i} \frac{1}{\sum_{k=j}^{N} m_k}. \tag{G19}$$

APPENDIX H: DERIVATION OF $\lim_{\beta \to 0} \beta \cdot \langle K_1 \rangle$

Here we present the calculation of Eq. (69), which represent the high-temperature limit $\lim_{\beta \to 0} \beta \cdot \langle K_1 \rangle$. From Eqs. (47), (57), and (61), we have

$$\beta \langle K_1 \rangle = \frac{\mu_1}{2} \frac{\int \frac{1}{\sqrt{1-\mu_2 C_{12}^2}} e^{-\beta U(\varphi)} d^2\varphi}{\int \sqrt{1-\mu_2 C_{12}^2}\, e^{-\beta U(\varphi)} d^2\varphi} \tag{H1}$$

for the double pendulum. Here $C_{12} = \cos(\varphi_2 - \varphi_1)$, and the region of integration is $0 \leqslant \varphi_i < 2\pi$, $i = 1, 2$.

Considering the limit $\beta \to 0$ on both sides, we have

$$\lim_{\beta \to 0} \beta \cdot \langle K_1 \rangle = \frac{\mu_1}{2} \frac{\int \frac{1}{\sqrt{1-\mu_2 C_{12}^2}} d^2\varphi}{\int \sqrt{1-\mu_2 C_{12}^2}\, d^2\varphi}$$
$$= \frac{\mu_1}{2} \frac{K(\sqrt{\mu_2})}{E(\sqrt{\mu_2})}, \tag{H2}$$

where $K(k)$ and $E(k)$ are the complete elliptic integrals of the first and second kind, respectively.

APPENDIX I: POINCARÉ SURFACE OF SECTION

Here, we explain the definition of the Poincaré surface of section used in Fig. 14. A unique correspondence from a point (φ_2, p_2) on the surface to a single point $(\varphi_1, \varphi_2, p_1, p_2)$, in the phase space is necessary. We set two conditions $H(\varphi, p) = E$

and $\varphi_1 = 0$, which reduces the four-dimensional phase space to a two-dimensional space (φ_2, p_2). Let us specify a point (φ_2, p_2) on the Poincaré surface.

For systems including a double pendulum, the energy is of the form

$$\tfrac{1}{2}{}^t p A^{-1} p + U(\varphi_1, \varphi_2) = E. \tag{I1}$$

Let us express matrix A as

$$A = \begin{pmatrix} A_1 & A_2 \\ A_2 & A_3 \end{pmatrix}. \tag{I2}$$

By substituting this into Eq. (I1) and the straightforward calculation, we get

$$(A_3 p_1 - A_2 p_2)^2 = \det A \left\{ 2A_3 [E - U(\varphi_1, \varphi_2)] - p_2^2 \right\}. \tag{I3}$$

Hence, point (φ_2, p_2) corresponds to a unique point $(\varphi_1, \varphi_2, p_1, p_2)$ under $E = \text{const}$, and we must specify the sign of $A_3 p_1 - A_2 p_2$. Let us take a positive sign; then, the Poincaré surface of the section is defined as

$$\begin{aligned} \varphi_1 &= 0, \\ A_3 p_1 - A_2 p_2 &> 0. \end{aligned} \tag{I4}$$

In the case of a double pendulum, the last condition is equivalent to

$$\mu_2 \ell_2^2 p_1 - \mu_2 \ell_1 \ell_2 p_2 \cos\varphi_2 > 0 \tag{I5}$$

by substituting $\varphi_1 = 0$. For $\ell_1 = \ell_2$, this condition yields

$$p_1 - p_2 \cos\varphi_2 > 0, \tag{I6}$$

as shown in the caption of Fig. 14.

Using

$$\dot{\varphi} = A^{-1} p, \tag{I7}$$

we can convert the condition in Eq. (I4) in terms of $\dot{\varphi}$. Since

$$A_3 p_1 - A_2 p_2 = \dot{\varphi}_1 \cdot \det A, \tag{I8}$$

and the kinetic energy and matrix A are positive definite, we can consider

$$\varphi_1 = 0, \quad \dot{\varphi}_1 > 0 \tag{I9}$$

as the surface of the section.

[1] G. Galilei, *Dialogues Concerning Two New Sciences* (Lodewijk Elzevir, Leluven, 1638).
[2] H. Goldstein, *Classical Mechanics*, 2nd ed. (Addison-Wesley, Boston, 1980).
[3] D. Bernoulli, Comment. Acad. Sci. Imper. Petropol. **6**, 108 (1738).
[4] D. Bernoulli, Comment. Acad. Sci. Imper. Petropol. **7**, 162 (1740).
[5] J. T. Cannon and S. Dostrovsky, *The Evolution of Dynamics: Vibration Theory from 1687 to 1742* (Springer-Verlag, Berlin, 1981).
[6] A. J. Lichtenberg and M. A. Lieberman, *Regular and Chaotic Dynamics* (Springer, Berlin, 1992).
[7] E. Ott, *Chaos in Dynamical Systems*, 2nd. ed. (Cambridge University Press, Cambridge, UK, 2002).
[8] M. Tabor, *Chaos and Integrability in Nonlinear Dynamics: An Introduction* (Wiley Interscience, New York, 1989).
[9] T. Shinbrot, C. Grebogi, J. Wisdom, and J. A. Yorke, Am. J. Phys. **60**, 491 (1992).
[10] T. Stachowiak and T. Okada, Chaos, Solitons Fractals **29**, 417 (2006).
[11] M. Z. Rafat, M. S. Wheatland, and T. R. Bedding, Am. J. Phys. **77**, 216 (2009).
[12] H. R. Dullin, Z. Phys. B: Condens. Matter **93**, 521 (1994).
[13] T. Stachowiak and W. Szumiński, Phys. Lett. A **379**, 3017 (2015).
[14] A. V. Ivanov, Regular Chaotic Dyn. **4**, 104 (1999).
[15] A. V. Ivanov, J. Phys. A: Math. Gen. **34**, 11011 (2001).
[16] A. V. Ivanov, Regular Chaotic Dynam. **5**, 329 (2000).
[17] A. V. Ivanov, Regular Chaotic Dynam. **6**, 53 (2001).
[18] Y. Oyama and T. Yanagita, Abstr. Meet. Phys. Soc. Jpn. **53**, 733 (1998).
[19] N. Saitoh, Y. Oyama, and T. Yanagita, Abstr. Meet. Phys. Soc. Jpn. **54**, 670 (1999).
[20] N. Saitoh and T. Yanagita, Abstr. Meet. Phys. Soc. Jpn. **55**, 207 (2000).
[21] R. C. Tolman, Phys. Rev. **11**, 261 (1918).
[22] R. C. Tolman, *The Principles of Statistical Mechanics* (Oxford University Press, Oxford, 1938).
[23] R. Kubo, H. Ichimura, T. Usui, and N. Hashitsume, *Statistical Mechanics* (North Holland, Amsterdam, 1990).
[24] T. Konishi and T. Yanagita, J. Stat. Mech. (2009) L09001.
[25] B. Leimkuhler and S. Reich, *Simulating Hamiltonian Dynamics* (Cambridge University Press, Cambridge, UK, 2004).
[26] Chemistry at Harvard Macromolecular Mechanics (CHARMM), http://www.charmm.org/.
[27] F. J. Vesely, Am. J. Phys. **81**, 537 (2013).
[28] H. Yoshida, Phys. Lett. A **150**, 262 (1990).
[29] NIST Digital Library of Mathematical Functions, https://dlmf.nist.gov/.
[30] T. Konishi and T. Yanagita, J. Stat. Phys. **190**, 15 (2023).
[31] W. Kuhn, Kolloid Z. **68**, 2 (1934).
[32] W. Kuhn and H. Kuhn, J. Colloid Sci. **3**, 11 (1948).
[33] H. A. Kramers, J. Chem. Phys. **14**, 415 (1946).
[34] M. Fixman, Proc. Natl. Acad. Sci. USA **71**, 3050 (1974).
[35] M. Fixman and J. Kovac, J. Chem. Phys. **61**, 4950 (1974).
[36] M. Mazars, Phys. Rev. E **53**, 6297 (1996).
[37] M. Doi and S. Edwards, *The Theory of Polymer Dynamics* (Clarendon Press, Oxford, 1988).
[38] M. Doi, *Introduction to Polymer Physics* (Oxford University Press, Oxford, 1996).
[39] G. R. Strobl, *The Physics of Polymers: Concepts for Understanding Their Structures and Behavior* (Springer, Berlin, 1997).
[40] G. R. Siegert, R. G. Winkler, and P. Reineker, Z. Naturforsch. A **48**, 584 (1993).
[41] T. Niiyama, Y. Shimizu, T. R. Kobayashi, T. Okushima, and K. S. Ikeda, Phys. Rev. Lett. **99**, 014102 (2007).

[42] L. Openov and A. Podlivaev, Phys. Solid State **50**, 1195 (2008).
[43] L. Boltzmann, Nature **51**, 413 (1895).
[44] J. H. Jeans, Lond. Edinb. Dubl. Philos. Mag. J. Sci. **6**, 279 (1903).
[45] J. H. Jeans, Lond. Edinb. Dubl. Philos. Mag. J. Sci. **10**, 91 (1905).
[46] N. Nakagawa and K. Kaneko, Phys. Rev. E **64**, 055205(R) (2001).
[47] G. Benettin, L. Galgani, and A. Giorgilli, Phys. Lett. A **120**, 23 (1987).
[48] G. Benettin, L. Galgani, and A. Giorgilli, Commun. Math. Phys. **121**, 557 (1989).
[49] G. Benettin, Prog. Theor. Phys. Suppl. **116**, 207 (1994).
[50] T. Konishi and T. Yanagita, J. Stat. Mech. (2010) P09001.
[51] T. Konishi and T. Yanagita, J. Stat. Mech. (2016) 033201.
[52] J. M. Sanz-Serna and M. P. Calvo, *Numerical Hamiltonian Problems* (Dover, Mineola, NY, 2018).
[53] A. Pikovsky and A. Politi, *Lyapunov Exponents: A Tool to Explore Complex Dynamics* (Cambridge University Press, Cambridge, UK, 2016).
[54] I. Shimada and T. Nagashima, Prog. Theor. Phys. **61**, 1605 (1979).
[55] The term "linear" is used because the "momentum" $m\dot{q}$ is often called as the "linear momentum".
[56] D. Landau and K. Binder, *A Guide to Monte Carlo Simulations in Statistical Physics* (Cambridge University Press, Cambridge, UK, 2005).
[57] M. E. J. Newman and G. T. Barkema, *Monte Carlo Methods in Statistical Physics* (Oxford University Press, Oxford, 1999).